Modeling Two-Phase Flow with Hysteresis: Comparative Study of Hysteresis Models and Application

Abdellah Amri, Zakaria Saâdi, Rachid Ababou

HAL Id: hal-04379373
https://hal.science/hal-04379373

Modeling two-phase flow with hysteresis: comparative study of hysteresis models and application

Amri Abdellah[1,2], Zakaria Saâdi[1*] and Rachid Ababou[2]

[1] PSE-ENV/SEDRE/UEMIS, Institut de Radioprotection et de Sûreté Nucléaire (IRSN), 31 Av. de la Division Leclerc, Fontenay-aux-Roses, 92262, France.
[2] Institut de Mécanique des Fluides de Toulouse (IMFT), 2 Rue du Prof. Camille Soula, Toulouse, 31400, France.

*Corresponding author(s). E-mail(s): zakaria.saadi@irsn.fr;
Contributing authors: abdellahamri7@gmail.com;
rachidababou@gmail.com;

Abstract

Drainage (drying) and imbibition (wetting) cycles are expected in many applications involving subsurface flows, such as underground CO2 storage, hydrocarbon extraction and production, and deep geological disposal of radioactive waste (particularly in the potential production of hydrogen due to corrosion and radiolysis). In the presence of imbibition/drainage cycles, the two-phase constitutive relations between water saturation, capillary pressure and relative permeability to liquid and gas, cannot be represented by simple one-to-one functions: they depend on the history of wetting/drying processes. Recent numerical and experimental studies highlight the importance of hysteresis and its effect on two-phase flows in porous media. In this study, an extensive critical review of conceptual hysteretic models is first presented. The performance of these models is evaluated and tested from a theoretical point of view based on their assumptions, and by confronting them with measured data for various porous materials extracted from the literature (cement, sands, Bentonite MX80). The advantages and disadvantages of the different hysteretic constitutive models are discussed. Finally, we implement the five hysteresis models in the iTOUGH2 code, and we develop a numerical simulation of a two-phase flow experiment with immiscible

fluids at the laboratory scale (meters), in order to compare the flow results obtained with or without hysteresis, and also, with or without capillary entrapment. The results highlight the need to take into account hysteresis in the modeling of multiphase porous media flows, especially when they are subjected to drying-wetting cycles. It is suggested that the model of Beriozkin and Mualem 2018 should be preferred both from a theoretical standpoint and for its computational advantages.

Highlights

- Quantitative assessment of several significant and representative conceptual models for hysteretic two-phase flow in porous media.
- Identification of best hysteresis model in terms of physical parametrization, accuracy, and ease of implementation.
- Gas entrapment in hysteresis models is found to be essential for accurate simulations of gas-liquid flow in porous media.

1 Introduction

Accurate characterisation of the relationships of hydraulic properties is essential to understanding and modeling multi-phase flow in porous media. These relationships are subject to the hysteresis phenomenon during drying and wetting cycles. Various models have been used over the years to describe the hysteretic capillary-saturation relationships. A detailed overview of existing hysteresis models can be found in Mualem, Beriozkin (2009), Zhang et al. (2014) and Albers (2014). Many studies (Lenhard et al. (1989), Doughty (2007), Zhang (2014), Cihan et al. (2017)) have highlighted the necessity of taking into account hysteresis phenomena in the modeling of multiphase transport in porous media.

For example, Parker, Lenhard (1987) and Lenhard, Parker (1987) produced two successive articles dealing with hysteresis in the capillary water retention curve $P_c(S)$ and in the liquid-gas relative permeability curves $k_{rL}(S)$ and $k_{rG}(S)$. A hysteretic model based on the concept of non-wetting phase entrapment was proposed, using the Scott (1983) scaling technique. After a series of publications, Lenhard (1992) showed that there is a significant difference in fluid saturations between hysteretic and non-hysteretic simulations of NAPLs (Non-Aqueous Phase Liquids) distribution in the vadose zone. Doughty (2007) introduced the concept of non-wetting phase entrapment saturation in the hysteresis model of Mualem (1984) in a simple manner, introducing the formula

of Land (1968) in the unsaturated Van Genuchten-Mualem ("VGM") formulation (Van Genuchten (1980)). The model was extended to gas and water permeabilities using the Parker, Lenhard (1987) formulation. The Doughty (2007) hysteretic model was implemented in the iTOUGH2 code, and illustrated with an example simulation of injection of supercritical carbon dioxyde in a saline aquifer, where the effect of hysteresis is well demonstrated. Zhang et al. (2014) conducted a comparative study of several models, including the empirical models of Rubin (1967), Feng, Fredlund (1999), Braddock et al. (2001), Li (2005), and the conceptual models of Mualem (1974) and Mualem (1984). They showed that the conceptual models are more accurate than the empirical ones for predicting wetting and drying cycles of moisture dynamics in cementitious materials.

On the other hand, Cihan et al. (2017) developed a hysteresis model based on relating macroscopic variables to the microscopic properties of the porous media, including void distribution and connectivity function. Using an intermediate-scale laboratory experiment of non-wetting fluid injection in a porous medium initially saturated with a glycerol-water mixture, they concluded that their hysteresis model predicts well the non-wetting plume migration and its distribution during and after injection, compared to the non-hysteretic model. More recently, Beriozkin, Mualem (2018) showed that the Parker, Lenhard (1987) model for the capillary water retention curve $P_c(S_l)$ has the undesirable property of "non parallelism" . That is, the two scanning curves departing from the main drying curve and the first drying curve are not "parallel". Consequently, they are not accompanied by the same increase in saturation. In other words, the two primary wetting processes, predicted by the Parker, Lenhard (1987) model are described by non-parallel effective saturation curves, displaying different increments of water content during the same changes of capillary pressure. Thus, the Parker, Lenhard (1987) model introduces an inconsistency into the apparent saturation model, although on the other hand, it is practical because it uses an available computational tool (i.e. Land's 1968 formula). On the other hand, Beriozkin, Mualem (2018) used the linear law for non-wetting phase entrapment applied to the Mualem (1974) model to derive 6 equations of scanning curves stemming from the main curves.

In conclusion, choosing the appropriate model of hysteresis (and of non-wetting phase entrapment) appears to be a challenging task in modeling multiphase flow in porous media.

In the present study, we perform a review and comparison between the well-known physically-based conceptual models in the literature. The models are tested on a wide range of porous media. The representation of non-wetting phase entrapment is discussed, and a general algorithm for modeling hysteresis is provided, with a discussion of the important hyper-parameters. Finally, the intermediate-scale laboratory experiment of Soltrol-220 injection into a slab of sandy porous medium fully saturated with a glycerol-water mixture (Trevisan et al. (2014)) is simulated with and without hysteresis.

2 Brief description of some conceptual hysteresis models

Hysteresis models can be classified into two categories, empirical and conceptual. The empirical models are based on fitting hyper-parameters from the two scanning curves in order to predict any scanning curve. These models are not taken into account in this study due to pumping errors (PE) resulting from the non-closure of scanning hysteresis loops associated with spurious cyclic oscillations as reported in Zhang et al. (2014). These empirical models may require an additional measured scanning curve of higher order for their validation. The conceptual models are generally based on independent and dependent domain theory which has been first introduced in porous media flow by Poulovassilis (1962) . This theory has been developed by Preisach (1935) to describe ferromagnetic hysteresis. Conceptual models have been extended in many recent studies to take into account the capillary entrapment phenomena. In this section we present an exhaustive critical review of a wide range of conceptual hysteresis models based on Mualem (1974), Mualem (1984), Haverkamp et al. (2002), Doughty (2007), and Beriozkin, Mualem (2018).

2.1 Empirical hysteresis models without non-wetting phase entrapment

The classical models of hysteresis are based on interpolating values of scanning curves from main curves. In this review we focus on hysteresis models derived from two theories. The first one is the domain theory which combines models based on the dependent domain theory from Mualem (1974) and the independent domain theory from Mualem (1984). The second theory is based on the rational extrapolation of Parlange (1976), also adopted later by Haverkamp et al. (2002).

2.1.1 Mualem 1974 model

According to the domain theory in soil physics, the porous media can be presented by a bi-variate pore water distribution function $f(\bar{r}, \bar{\rho})$ where :

$$\bar{r} = \frac{r(P_c) - r(P_{c,min})}{r(P_{c,max}) - r(P_{c,min})}$$

and

$$\bar{\rho} = \frac{\rho(P_c) - \rho(P_{c,min})}{\rho(P_{c,max}) - \rho(P_{c,min})}$$

are two normalized pore radius parameters varying from 0 to 1 as capillary pressure P_c varies from $P_{c,min}$ to $P_{c,max}$. They can be interpreted respectively as the radius of pore body and the radius of pore neck, following representation of hysteresis phenomena as the ink-bottle effect as described in M'Jahad (2012). Following this representation of pore size distribution, the water saturation is obtained by integration of the pore water distribution function, as

follows:

$$S(P_c) = \int_{\bar{r}\in I_{\bar{r}(P_c)}} \int_{\bar{\rho}\in I_{\bar{\rho}(P_c)}} f(\bar{r}, \bar{\rho}) \, d\bar{\rho} \, d\bar{r} \tag{1}$$

Mualem (1974) assumed that each group of pores is independent of its neighbors. More precisely, this assumption stipulates that pore neck size is totally independent from pore body size and the bi-variate function can be expressed as the product of two independent functions $f(\bar{r}, \bar{\rho}) = h(\bar{r}) \times l(\bar{\rho})$. The water saturation $S(P_c)$ at a given capillary pressure can be obtained by integration of pore water distribution function over specific intervals, $I_{\bar{\rho}(P_c)}$ and $I_{\bar{r}(P_c)}$, as follows:

$$S(P_c) = \int_0^{\bar{r}(P_c)} \int_0^{\bar{\rho}(P_c)} f(\bar{r}, \bar{\rho}) \, d\bar{\rho} d\bar{r} = \int_0^{\bar{r}(P_c)} \int_0^{\bar{\rho}(P_c)} h(\bar{r}) \times l(\bar{\rho}) \, d\bar{\rho} d\bar{r} \tag{2}$$

In order to illustrate the drying and wetting processes, and to derive scanning curves equations, Mualem (1974) used the diagram shown in figure (1) and figure (2). We have drawn these figures in such a way that they explicitly show the drying and wetting cycles as represented by the independent domain theory.
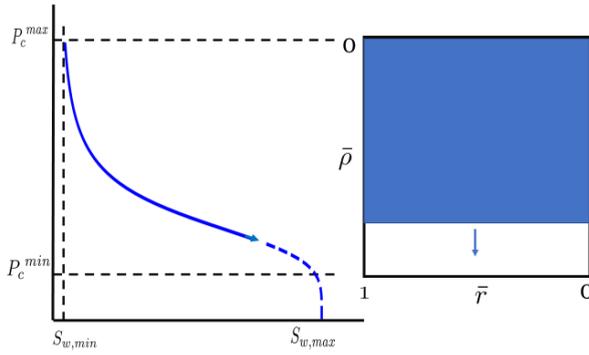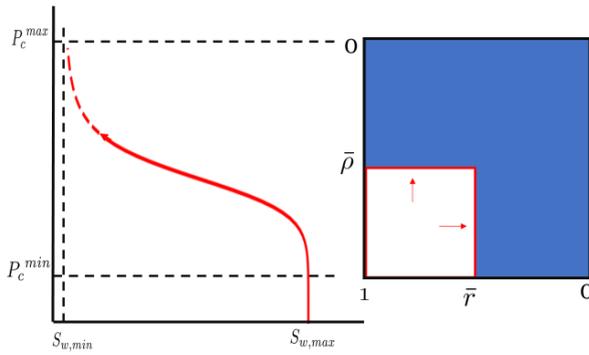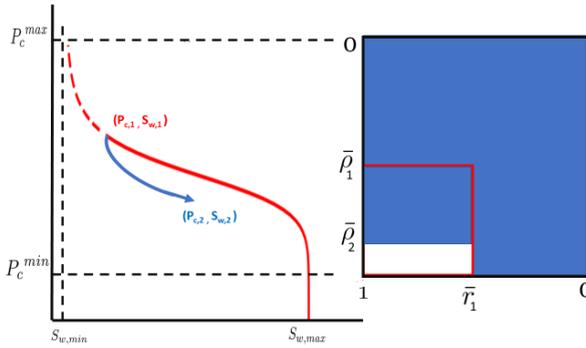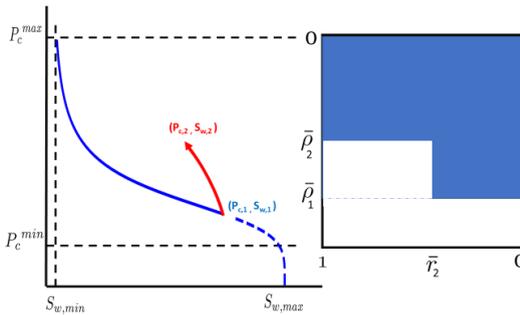
(a) Main wetting curve $P_c(S)$

(b) Main drying curve $P_c(S)$

Figure 1: Schematic representation of wetting/drying processes based on the independent domain theory diagram (Mualem (1974)): (a) main wetting; (b) main drying.

(a) First wetting curve departing from main drying curve

(b) First drying curve departing from main wetting curve

Figure 2: Schematic representation of wetting/drying processes based on the independent domain theory diagram (Mualem (1974)): (a) first wetting scanning curve; (b) first drying scanning curve.

In these two diagrams, the process of drying and wetting of pores is governed by two assumptions:

- For the drying process from $P_c(\bar{R})$ to $P_c(\bar{R} - d\bar{R})$ only the groups of pores characterized by $\bar{R} \leq \bar{r} \leq 1$ and $\bar{R} - d\bar{R} \leq \bar{\rho} \leq \bar{R}$ are drained,
- For the wetting process from $P_c(\bar{R})$ to $P_c(\bar{R} + d\bar{R})$ all the groups of pores characterized by $\bar{R} \leq \bar{\rho} \leq \bar{R} + d\bar{R}$ are filled.

Based on these assumptions, Mualem (1974) derived an explicit formulation of any scanning curve order (first drying, second wetting, third drying..). Let $S_{N,d}(P_c)$ (resp. $S_{N,w}(P_c)$) be the unknown saturation for the Nth drying (resp. Nth wetting) curve from the Nth turning point $S_{tp,N}(P_{c,N})$, then $S_{N,d}(P_c)$ (resp. $S_{N,w}(P_c)$) can be expressed by:

$$S_{N,d}(Pc) \;=\; S_{tp,N}(P_{c,N}) - \int_{\bar{r}(P_c)}^{1} \int_{\bar{\rho}(P_{c,N})}^{\bar{\rho}(P_c)} h(\bar{r}) \times l(\bar{\rho}) \, d\bar{\rho} d\bar{r} \qquad (3)$$

$$S_{N,w}(Pc) \;=\; S_{tp,N}(P_{c,N}) + \int_{0}^{1} \int_{\bar{\rho}(P_c)}^{\bar{\rho}(P_{c,N})} h(\bar{r}) \times l(\bar{\rho}) \, d\bar{\rho} d\bar{r} \qquad (4)$$

From the integration of the pore water distribution based on equations (3) and (4), the Nth scanning path for the drying and wetting process can be written explicitly as :

$$S_{N,d}(P_c) \;=\; \begin{cases} S_{tp,N}(P_{c,N}) - (S_w(P_{c,N}) - S_w(P_c))(\frac{S_{max,w} - S_d(P_c)}{S_{max,w} - S_w(P_c)}) & \text{if } P_c \leq P_{c,N-1} \\ S_{N-2,d}(P_c) & \text{if } P_c \geq P_{c,N-1} \end{cases}$$
$$(5)$$

$$S_{N,w}(P_c) \;=\; \begin{cases} S_{tp,N}(P_{c,N}) + (S_w(P_c) - S_w(P_{c,N}))(\frac{S_{max,w} - S_d(P_{c,N})}{S_{max,w} - S_w(P_{c,N})}) & \text{if } P_c \geq P_{c,N-1} \\ S_{N-2,w}(P_c) & \text{if } P_c \leq P_{c,N-1} \end{cases}$$
$$(6)$$

where $S_{0,w} = S_w$ (resp $S_{0,d} = S_d$) is the main wetting (resp drying) curve, and $S_{max,w}$ is the maximum water saturation for a complete wetting process starting with an initially dry porous medium.

Equations (5) and (6) define scanning curves of any order as illustrated in figure (3), where a series of scanning curves were plotted based on the hysteretic model of Mualem (1974) and the Van Genuchten (VG) formulation (Eq. (7), Van Genuchten (1980)) for the main curves with parameters $n_w = n_d = 2.145$, $\alpha_d = 2.61 \times 10^{-4} [Pa^{-1}]$, $\alpha_w = 9.16 \times 10^{-4} [Pa^{-1}]$, $S_{ls} = 1.0$, and $S_{lr} = 0$.

$$\frac{S(P_c) - S_{lr}}{S_{ls} - S_{lr}} \;=\; [1 + (\alpha P_c)^n]^{-m} \qquad (7)$$

The hysteretic turning points are $P_{c,1} = 1.4 \times 10^4$ Pa, $P_{c,2} = 600$ Pa, $P_{c,3} = 9 \times 10^3$ Pa, and $P_{c,4} = 2 \times 10^3$ Pa in figure (3.a), and $P_{c,1} = 900$ Pa, $P_{c,2} = 1.4 \times 10^4$ Pa, $P_{c,3} = 1.1 \times 10^3$ Pa, $P_{c,4} = 9 \times 10^3$ Pa in figure (3.b).
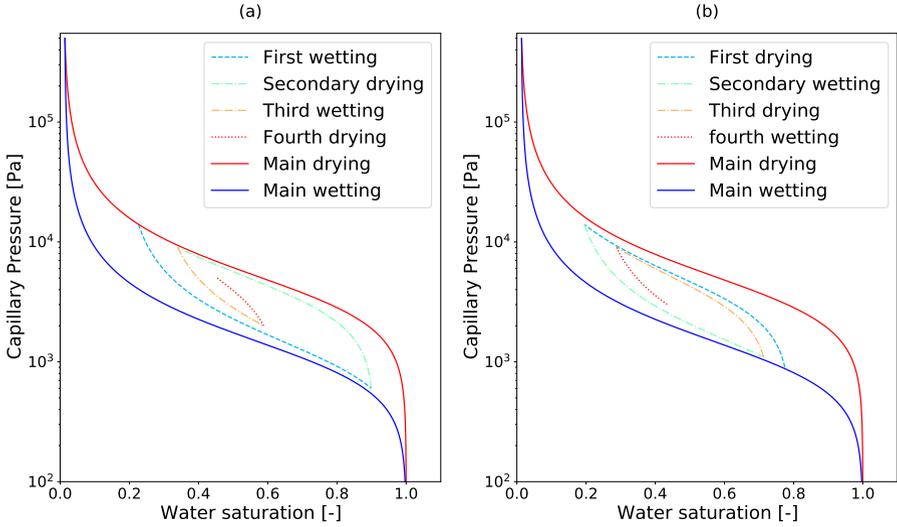
Figure 3: Schematic illustration of soil water hysteresis with the independent domain theory of Mualem (1974): (a) continuous sequence of scanning curves departing from the main drying curve; (b) continuous sequence of scanning curves departing from the main wetting curve.

2.1.2 Mualem 1984 model (dependent domain theory)

The previous model of Mualem (1974) assumed that the drying and wetting processes in pores are independent of the state of saturation of neighboring pores, which is not the case in a real porous medium. To take into account this dependency, Mualem (1984) introduced different factors in order to take into account the portion of drainable pores in a new model, called the universal model, corresponding to the 'dependent domain' theory of Mualem (1984). This new model integrates (involves) only one dependent factor P_d which can be related to the pore blockage against the non-wetting phase (air).

The model proposes the following formulation for the N-th wetting (resp, N-th drying) curve $S_{N,w}(P_c)$ (resp $S_{N,d}(P_c)$) departing from the N-th turning point $S_{tp,N}(P_{c,N})$. First, we have:

$$S_{N,w}(P_c) =$$

$$\begin{cases} S_{tp,N}(P_{c,N}) + P_d(S_{tp,N}(P_{c,N})) \times (S_w(P_c) - S_w(P_{c,N}))(\frac{S_{max,w} - S_w(P_{c,N})}{S_{max,w}}) \\ S_{N-2,w}(P_c) \end{cases}$$

$$(8)$$

where the first equation is for $P_c \geq P_{c,N-1}$, and the second equation is for $P_c \leq P_{c,N-1}$. And secondly, we have:

$$S_{N,d}(P_c) =$$
$$\begin{cases} S_{tp,N}(P_{c,N}) - P_d(S_{N,d}(P_c)) \times (S_w(P_{c,N}) - S_w(P_c))(\frac{S_{max,w} - S_w(P_c)}{S_{max,w}}) \\ S_{N-2,d}(Pc) \end{cases} \quad (9)$$

where, again, the first equation is for $P_c \leq P_{c,N-1}$, and the second equation is for $P_c \geq P_{c,N-1}$. In these equations, $P_d(S)$ is defined as:

$$P_d(S) = \frac{(S_{max,w} - S) \times S_{max,w}}{(S_{max,w} - S_w(P_c^*))^2}$$

and P_c^* is defined by the relation: $S_d(P_c^*) = S$.

Note that equation (9) provides an implicit solution for the N-th drying curve; therefore, an iterative method is required to compute $S_{N,d}(P_c)$.
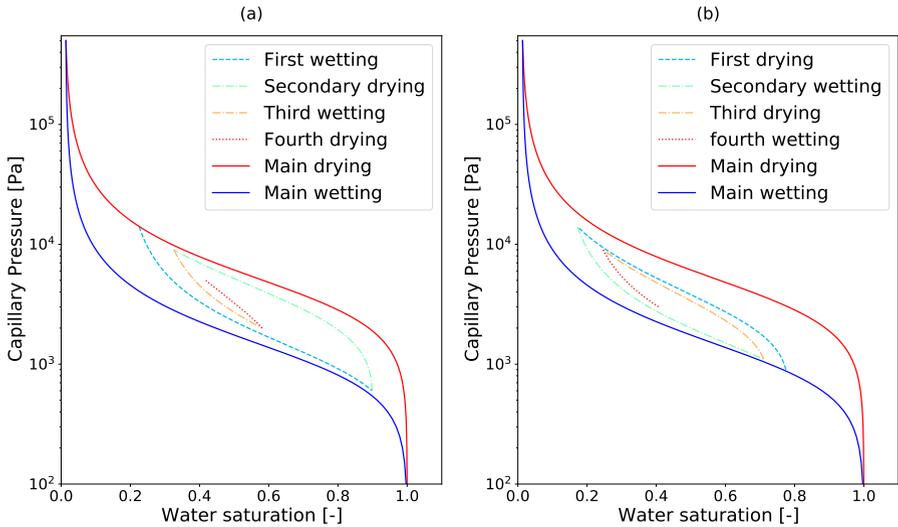

Figure 4: Schematic illustration of soil water hysteresis with the dependent domain theory of Mualem (1984): (a) continuous sequence of scanning curves departing from the main drying curve; (b) continuous sequence of scanning curves departing from the main wetting curve. Idem Van Genuchten parameters of main curves in figure (3).

Comparing the independent and dependent domain theories of Mualem (1974) and Mualem (1984) as illustrated in figure (3) and figure (4), respectively, it can be seen that, for the same turning points, the dependent domain theory leads to a higher desaturation than the independent domain theory.

2.1.3 Haverkamp et al. 2002 geometrical scaling model

Based on the theoretical model of Parlange (1976), Haverkamp et al. (2002) derived geometrical scaling conditions for defining a hysteresis model. The model assumes that all the main curves and the scanning curves have the same normalized Van Genuchten formulation (Eq. (7)). For the Nth scanning curve, the normalized water saturation can be defined as:

$$\bar{S}_{N,p}(P_c) = \frac{S_{N,p}(P_c) - S_{lr,N,p}}{S_{ls,N,p} - S_{lr,N,p}} = [1 + (\alpha_{N,p} \times P_c)^{n_{N,p}}]^{m_{N,p}} \quad (10)$$

where $\bar{S}_{N,p}(P_c)$ (resp $S_{N,p}(P_c)$) is the normalized water saturation (resp. the actual water saturation) for the Nth scanning curve with respect to the drying path (p=d) and wetting path (p=w). Note here that the symbol "p" is used as a path label (drying or wetting). Parameters $S_{ls,N,p}$, $S_{lr,N,p}$, $n_{N,p}$, $m_{N,p}$, $\alpha_{N,p}$ are the VG-parameters corresponding to the N-th scanning curve with respect to the path "p". The determination of the Nth scanning curves ($S_{ls,N,p}$, $n_{N,p}$, $m_{N,p}$, $\alpha_{N,p}$) from the main curves parameters ($S_{ls,0,p}$, $n_{0,p}$, $m_{0,p}$, $\alpha_{0,p}$) is based on the constitutive relationships as follows...

• All wetting and scanning curves have identical shape parameters:

$$n = n_{0,w} = n_{0,d} = n_{N,w} = n_{N,d} \quad (11a)$$

$$m = m_{0,w} = m_{0,d} = m_{N,w} = m_{N,d} \quad (11b)$$

• The pressure scale parameters of the main wetting and the main drying curves are related by :

$$\alpha_{0,w} = k \times \alpha_{0,d} \text{ where } k = \begin{cases} 2 & \text{if } m \times n > 1 \\ [1 + m \times n]^{\frac{1}{m \times n}} & \text{if } 0 < m \times n < 1 \end{cases} \quad (12)$$

• The closure of scanning curves implies that each curve joins the point of departure of its parent curve, which leads to the specific conditions $S_{ls,0,d} = S_{ls,0,w} = S_{ls,1,w} = S_{ls}$ and $S_{lr,0,d} = S_{lr,0,w} = S_{lr,1,d} = 0$.

• The pressure scale parameter for the N-th scanning curve is given by:

$$\alpha_{N,p} = \alpha_{0,p} \times [\frac{S_{ls}}{S_{ls,N,p} - S_{lr,N,p}}]^{\frac{-1}{m \times n}} \quad (13)$$

- The N-th scanning curve is defined in the range of the actual turning point $S_{tp,N}$ and the previous turning point $S_{tp,N-1}$. For example, for the first wetting process we have $S_{tp,N}$ is the turning point from the main drying curve and $S_{tp,N-1} = 1$. For the Nth wetting process departure from $(S_{tp,N}, P_{c,tr,N})$ and arrival to $(S_{tp,N-1}, P_{c,tr,N-1})$ for the path p process, where p=d for drying and p=w for wetting, the VGM parameters $S_{lr,N,p}$ and $S_{ls,N,p}$ are derived from the constitutive equations :

$$S_{ls,N,p} - S_{lr,N,p} = \frac{S_{tp,N} - S_{tp,N-1}}{S^*{}_{N,p}(P_{c,tr,N}) - S^*{}_{N,p}(P_{c,tr,N-1})} \tag{14a}$$

$$S^*{}_{N,p}(P_c) = [1 + k^{\epsilon_p} \times (\frac{S_{ls,N,p} - S_{lr,N,p}}{S_{ls,N-1,\bar{p}} - S_{lr,N-1,\bar{p}})})^{\frac{1}{m}} \times (\alpha_{k-1,\bar{p}} \times P_c)^n]^{-m} \tag{14b}$$

$$S_{lr,N,p} = \frac{S_{tp,N-1} \times S^*{}_{N,p}(P_{c,tr,N}) - S_{tp,N} \times S^*{}_{N,p}(P_{c,tr,N-1})}{S^*{}_{N,p}(P_{c,tr,N}) - S^*{}_{N,p}(P_{c,tr,N-1})} \tag{14c}$$

where $\epsilon_p=1$ for the wetting path (p=w) and $\epsilon_p=-1$ for the drying path (p=d). The $\bar{p}$ parameter designates the previous path of a scanning curve p (if p=d then $\bar{p}$=w and if p=w then $\bar{p}$=d). The system of equations (14) gives an implicit formulation of individual values of the parameters $S_{lr,N,p}$ and $S_{ls,N,p}$, first the difference $S_{ls,N,p} - S_{lr,N,p}$ is resolved from equations (14.a) and (14.b), and the individuals values are determined using equation (14.c).

Figure (5) shows a scanning curve departing from the main drying curve for the same VG-parameters used in figure (3) and figure (4), with turning points $P_{c,1} = 1.4 \times 10^4$ Pa, $P_{c,2} = 1600$ Pa. We note that the Haverkamp et al. (2002) model uses only one main curve to predict the hysteresis scanning curve.

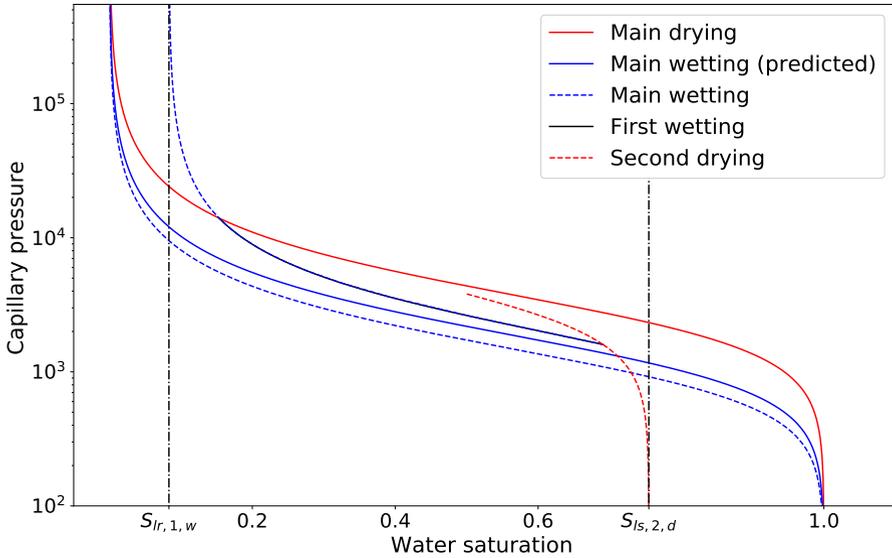**Figure 5**: Schematic illustration of soil water hysteresis with the geometrical scaling model of Haverkamp et al. (2002): continuous sequence of scanning curves departing from the main drying curve. Idem VG-parameters in figures (3) and (4).

The geometrical scaling of Haverkamp et al. 2002 gives an explicit expression for any scanning curve order. However, the main wetting and drying curves must verify equation (13), which is not always justified. Furthermore, an additional computational cost is induced by this model, due to the need for saving the Van Genuchten parameters for each scanning curve, as well as for all turning points.

2.2 Non-wetting phase entrapment with hysteretic models

In multiphase porous media, subject to wetting and drying cycles, the non-wetting fluid may be present as a disconnected phase due to capillary forces. Several experiments highlight this phenomenon and its impact in applications like CO_2 trapping: Hesse, Woods (2010), Krevor et al. (2011) and Trevisan et al. (2014). In this subsection, we discuss the different representations of non-wetting phase trapping and their implementation in different hysteresis models.

2.2.1 Non-wetting phase entrapment saturation

As reported through several experimental studies (e.g., Raeesi et al. (2014)) the amount of non-wetting phase entrapment saturation $S_{nw,r}^{\Delta}$ is highly correlated

to the initial non-wetting phase saturation $S_{nw,i}$. Land's formula (equation (15)) is the most widely used in existing hysteresis models:

$$S^{\Delta}_{nw,r} = \frac{1}{\frac{1}{S^{\Delta}_{nw,max}} + \frac{1}{1-S_{tp}} + \frac{1}{1-S_{lr}}} \tag{15}$$

where "Δ" stands for entrapment phenomenon and "nw,r" means non-wetting phase residual saturation. However, recent studies (Suzanne et al. (2003), Pentland et al. (2010)) reveal that the linear law of Aissaoui (1983) performs better to represent measured data. Aissaoui's formulation is an adaptation of the linear law of non-wetting phase entrapment. The non-wetting phase entrapment saturation $S^{\Delta}_{nw,r}$ increases linearly with the initial gas saturation $S_{g,i}$ before stabilizing (leveling of) to a maximal value of non-wetting phase entrapment saturation $S^{\Delta}_{nw,r,max}$:

$$S^{\Delta}_{nw,r} = \begin{cases} \frac{S^{\Delta}_{nw,r,max}}{S_{nw,c}} S_{nw,i} & \text{if } S_{nw,i} \leq S_{nw,c} \\ S^{\Delta}_{nw,r,max} & \text{if } S_{nw,i} \geq S_{nw,c} \end{cases} \tag{16}$$

The main parameter to represent the relation between initial now-wetting phase saturation and residual non-wetting phase entrapment is the maximal value of the non-wetting entrapped saturation $S^{\Delta}_{nw,r,max}$. This parameter depends on the type of fluid used (oil/air-water) and on the micro-structure of the porous medium. Doughty (2007) considered that $S^{\Delta}_{g,r,max}$ is a constant material property that depends only on the porosity ϕ according to Holtz's formula taken from the petroleum literature:

$$S^{\Delta}_{g,r,max} = -0.3136 \times ln(\phi) - 0.1334 \tag{17}$$

Suzanne et al. (2003) conducted a series of measurements on the maximum residual gas saturation for different porous media, and they concluded that the maximum gas entrapment saturation $S^{\Delta}_{g,r,max}$ cannot be predicted using porosity and permeability.

2.2.2 Lenhard and Parker 1987 models

In this subsection, we present the models of Parker, Lenhard (1987) and Lenhard, Parker (1987) for a two-phase system liquid-gas as described in Lenhard et al. (1991). A detailed description of hysteresis in three phase systems can be found in Lenhard et al. (1989) and Lenhard (1992). In order to account for the non-wetting phase entrapment, Parker, Lenhard (1987) introduced the notion of apparent liquid (water) saturation $\bar{S}_l^*(P_c)$, which can be expressed as the sum of the effective saturation of liquid ($\bar{S}_l$) and of the effective saturation of trapped gas ($\bar{S}_g^{ent}$), as follows:

$$\bar{S}_l^*(P_c) = \bar{S}_l(P_c) + \bar{S}_g^{ent}(P_c) \tag{18}$$

with:

$$\bar{S}_l(P_c) = \frac{S_l(P_c) - S_{lr}}{S_{ls} - S_{lr}}$$
$$\bar{S}_g^{ent}(P_c) = \frac{S_g^{ent}(P_c)}{S_{ls} - S_{lr}}$$

Based on a series of previous publications (Lenhard (1992), Kaluarachchi, Parker (1992)), Lenhard et al. (1992) presented a hysteresis model that was aimed at avoiding the effect of "pumping errors" in the hysteretic loops. The scanning curves were predicted based on the hysteresis model of Scott (1983). This new model applies the hysteresis model of Scott (1983) to the apparent liquid saturation $\bar{S}_l^*(P_c)$ and a linear representation of gas (non-wetting phase) entrapment in order to derive the effective liquid saturation $\bar{S}_l(P_c)$. The equation of the N-th scanning path "p" is determined by the most recent reversal point $(S^*_{tp,N}, P^*_{c,N})$ and the preceding reversal point $(S^*_{tp,N-1}, P^*_{c,N-1})$ as expressed by:

$$\bar{S}^*(P_c) = S^*_{tp,N-1} + (S^*_{tp,N} - S^*_{tp,N-1}) \frac{S_p^*(P_c) - S_p^*(P^*_{c,N-1})}{S_p^*(P^*_{c,N}) - S_p^*(P^*_{c,N-1})} \quad (19)$$

Lenhard, Parker (1987) assume that hysteresis in relative permeability relations is a result of non-wetting phase entrapment. The classical model of water and gas permeability of Mualem (1976) is expressed as follows:

$$k_{r,l}(\bar{S}_l) = \bar{S}_l^\tau \left[\frac{\Gamma(0, \bar{S}_l)}{\Gamma(0, 1)} \right]^2 \quad (20)$$

$$k_{r,g}(\bar{S}_l) = (1 - \bar{S}_l)^{\tau'} \left[\frac{\Gamma(\bar{S}_l, 1)}{\Gamma(0, 1)} \right]^2 \quad (21)$$

where $\bar{S}_l = \frac{S_l - S_{l,r}}{1 - S_{l,r}}$ is the effective water saturation, τ and τ' are dimensionless parameters related to the pore water connectivity (for liquid and gas phase, respectively), and Γ is the incomplete beta function.

In addition, Lenhard, Parker (1987) imposes a correction to the original Mualem formulation of the relative permeability to liquid (Eq.(20)) in order to take into account the non-wetting phase entrapment in the mobile fluid phases:

$$k_{r,l}(\bar{S}_l) = \bar{S}_l^\tau \left[\frac{\Gamma(0, \bar{\bar{S}}_l) - \frac{\bar{S}_{gt}}{1 - \bar{S}_{tp}} \times \Gamma(\bar{S}_{tp}, \bar{\bar{S}}_l)}{\Gamma(0, 1)} \right]^2 \quad (22)$$

$$k_{r,g}(\bar{S}_l) = (1 - \bar{\bar{S}}_l)^{\tau'} \left[\frac{\Gamma(\bar{\bar{S}}_l, 1)}{\Gamma(0, 1)} \right]^2 \quad (23)$$

where

- $\bar{S}_{gt} = \frac{S_{gt}(S_l - S_{tp})}{(1 - S_{l,r})(1 - S_{tp} - S_{gt})}$ is the effective trapped non-wetting phase saturation,
- $\bar{S}_{tp} = \frac{S_{tp} - S_{l,r}}{1 - S_{l,r}}$ is the effective turning point saturation,

- $\bar{\bar{S}}_l$ is the effective trapped non-wetting phase saturation, defined as the sum of the effective water saturation $\bar{S}_l$ and the effective trapped non-wetting phase saturation $\bar{S}_{gt}$.

We note that equation (22) is obtained in a general form and may be used in the next section in order to derive an expression for water permeability by using Land's formula for non-wetting phase entrapment. Adaptation may also be made for another use of $S_{g,r}^{\Delta}$-$S_{g,i}$ relationships.
The Lenhard, Parker (1987) model is a more realistic hysteresis model, it takes into account the phenomenon of non-wetting phase entrapment and its effect on the relative permeabilities. However, it involves intermediate operations to switch from apparent to effective water saturation.

2.2.3 Doughty 2007 model

Doughty (2007) applied the dependent domain theory of Mualem (1984) (see subsection 2.1.2) to a new formulation of Van Genuchten-Mualem (VGM) $P_c(S_l)$ relationship, accounting for entrapped gas saturation. The new formulation of the capillary pressure - liquid saturation relationship is described as follows :

$$P_c(S_l) = P_0^p \left[\left(\frac{S_l - S_{l,r}}{1 - S_{nw,r}^{\Delta} - S_{l,r}} \right)^{\frac{-1}{m^p}} - 1 \right]^{1-m^p} \tag{24}$$

where P_0^p, m^p, $S_{l,r}$ are the VGM parameters of the main wetting (p=w) and the main drying (p=d). The amount of entrapped non-wetting phase saturation $S_{g,r}^{\Delta}$ saturation depends on the the recent reversal point from drainage to imbibition S_{tp} and on the input parameter of maximum residual gas saturation $S_{g,r,max}^{\Delta}$, which is a characteristic of the porous medium, calculated from the main wetting curve and linearly given by Land formulation (Eq. (15)). Figure (6) shows hysteresis scanning curves derived from the main drying curve for the same parameters of VGM model in figure (3). The turning points are chosen to demonstrate the non-wetting phase entrapment; their numerical values are $P_{c,1} = 4.25 \times 10^3$ Pa, $P_{c,2} = 1 \times 10^3$ Pa, and $P_{c,3} = 3 \times 10^3$ Pa.
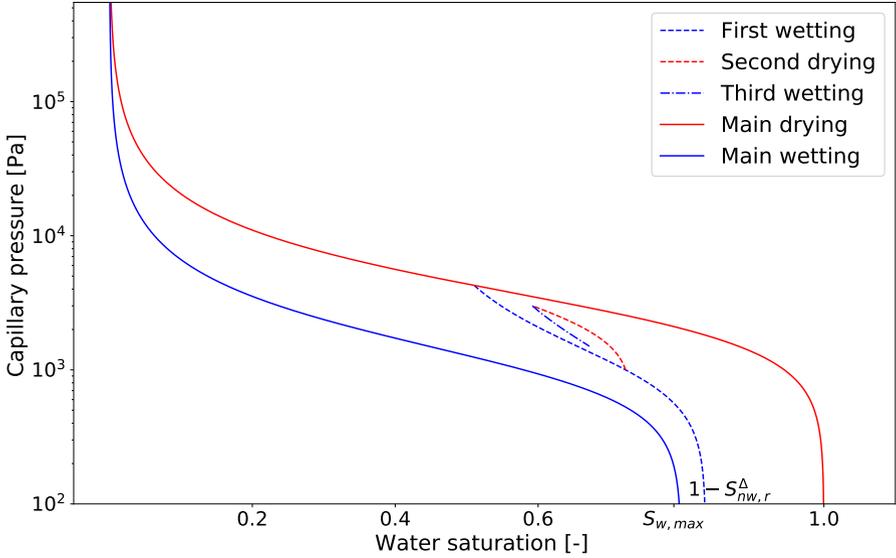
Figure 6: Schematic illustration of water-gas hysteresis using the Doughty (2007) model. The parameters of Van Genuchten model are the same as in the figure (3)

.

Doughty (2007) integrates equations (22) and (23) by using equation (24) in order to obtain explicit expressions for relative liquid permeability $k_{l,r}$ and relative gas permeability $k_{g,r}$, respectively:

$$k_{r,l}(\bar{S}_l) = \bar{S}_l^\tau \left[1 - (1 - \frac{\bar{S}_{gt}}{1 - \bar{S}_{tp}}) \times (1 - (\bar{S}_l + \bar{S}_{gt})^{\frac{1}{m}})^m - (\frac{\bar{S}_{gt}}{1 - \bar{S}_{tp}}) \times (1 - (\bar{S}_{tp})^{\frac{1}{m}})^m\right]^2 \tag{25}$$

$$k_{r,g}(\bar{S}_l) = (1 - (\bar{S}_l + \bar{S}_{gt}))^{\tau'} \times (1 - (\bar{S}_l + \bar{S}_{gt})^{\frac{1}{m}})^2 \tag{26}$$

This model was implemented by Doughty (2007) in the iTOUGH2 code (Finsterle et al. (2017)), with three scanning curves, first wetting, second drying, and semilog straight lines to approximate the third wetting curve as suggested by Niemi, Bodvarsson (1988).

The Doughty (2007) model uses a clever technique to represent the non-wetting phase entrapment saturation. This model as presented in Doughty (2007) and in Doughty (2013) has the disadvantage of approximating (linearizing) the $P_c(S_l)$ scanning curves near full water saturation (which is an important state in our studies on clay rock for radioactive waste disposal). In addition, the model is not based on empirical aspects; it only uses the Mualem (1984) model applied to a new scaling of the wetting curve after the first reversal point from a main drying path to the first wetting path.
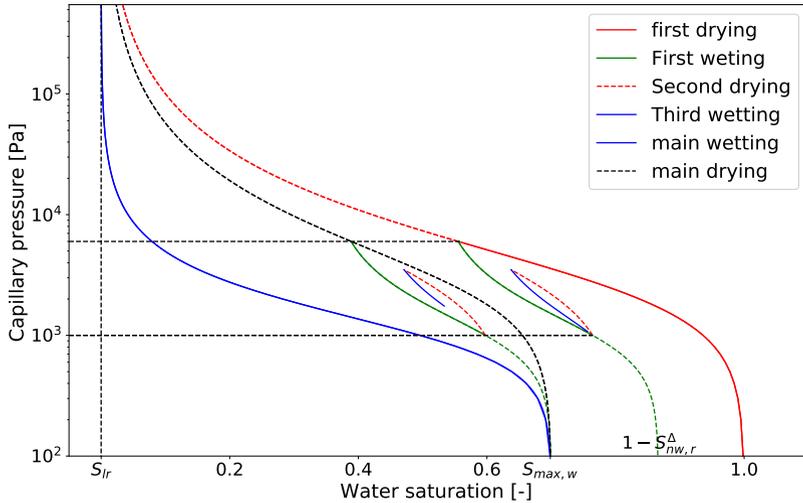
2.2.4 Beriozkin and Mualem 2018 model

Figure 7: Schematic representation of the hysteresis model of Beriozkin, Mualem (2018), with two parallel sequences of scans departing from the main wetting curve (MWC) and from the first drying curve (FDC).

Beriozkin, Mualem (2018) concluded that the hysteresis model with non-wetting phase entrapped suggested by Parker, Lenhard (1987) is based on invalid presumptions, and that the use of the entrapped non-wetting phase formula of Land (1968) implies non-parallelism between two primary wetting curves departing from the main drying and first drying curve as substantiated in Mualem (1974). The non-parallelism means that two paths of imbibition that start from the main drying and the first drying curve under an equal change of capillary pressure do not imply the same variation in saturation. Beriozkin, Mualem (2018) affirmed that the model of Parker, Lenhard (1987) presents a superfluous intermediate operation of predicting effective saturation from apparent saturation. Using the scaling technique of Mualem, Beriozkin (2009), Beriozkin, Mualem (2018) proposed a fully explicit equation to predict a desired scanning curve up to the third curve and expressed as follows:

- The primary wetting curve from the first turning point $(S_{tp,1}, P_{c,1})$:

$$S_{1,w}(P_c) = S_{max,w} - \frac{S_{max,w} - S_{tp,1}}{S_{max,w} - S_d(P_{c,1})}(S_{max,w} - S_w(P_c)) \qquad (27a)$$

- The secondary drying curve from the second turning point $(S_{tp,2}, P_{c,2})$ is :

$$S_{2,d}(P_c) = S_{tp,1} + \frac{S_{max,w} - S_{tp,1}}{S_{max,w} - S_w(P_{c,1})} \frac{S_w(P_{c,2}) - S_w(P_{c,1})}{S_d(P_{c,2}) - S_d(P_{c,1})} (S_d(P_c) - S_d(P_{c,1})) \tag{27b}$$

- And the tertiary wetting curve departing from the third turning point $(S_{tp,3}, P_{c,3})$ is :

$$S_{3,w}(P_c) = S_{max,w} - \frac{S_{max,w} - S_{tp,1}}{S_{max,w} - S_w(P_{c,1})} \times [(S_{max,w} - S_w(P_{c,2})) +$$

$$\frac{S_d(P_{c,2}) - S_d(P_{c,3})}{S_w(P_{c,2}) - S_w(P_{c,3})} \frac{S_w(P_{c,2}) - S_w(P_{c,1})}{S_d(P_{c,2}) - S_d(P_{c,1})} (S_w(P_{c,2}) - S_w(P_c))] \tag{27c}$$

For scanning curves departing from the first drying curve ($S_{ls} = 1$), a parallel shift is used by adding to each scanning equation (Eq. (27a), Eq. (27b), and Eq. (27c)) a value of $1 - S_{max,w}$.

For a sequence of scanning curves departing from the main wetting curve, the scanning curves are given as follows...

- The primary drying curve from the first turning point $(S_{tp,1}, P_{c,1})$:

$$S_{1,d}(P_c) = \frac{S_{tp,1}}{S_d(P_{c,1})} S_w(P_c) \tag{28a}$$

- The secondary wetting curve departing from the second turning point $(S_{tp,2}, P_{c,2})$ is :

$$S_{2,w}(P_c) = S_{tp,1} - S_{tp,1} \frac{S_d(P_{c,1}) - S_d(P_{c,2})}{S_{tp,1} - S_w(P_{c,2})} \frac{S_{tp,1} - S_w(P_c)}{S_d(P_{c,1})} \tag{28b}$$

- And the tertiary drying curve departing from the third turning point $(S_{tp,3}, P_{c,3})$ is :

$$S_{3,d}(P_c) = \frac{S_{tp,1}}{S_d(P_{c,1})} \times [S_d(P_{c,2}) +$$

$$\frac{S_d(P_{c,1}) - S_d(P_{c,2})}{S_{tp,1} - S_w(P_{c,2})} \frac{S_w(P_{c,3}) - S_w(P_{c,2})}{S_d(P_{c,3}) - S_d(P_{c,2})} (S_w(P_c) - S_w(P_{c,2}))] \tag{28c}$$

The explicit equations (28) are applied here to normalized water saturations, with $S_{max,d} = 1.0$ and $S_{l,r} = 0$ (the maximum drying saturation is unity and the residual liquid saturation is zero).

This hysteresis model of Beriozkin, Mualem (2018) gives an explicit formulation of the scanning curve without the need of iterative solution to compute

the value in the scanning curves at each grid block and at each iteration. This may be very promising for reducing the computational cost of hysteresis, as noted for instance by Doughty (2013). However, this model (Beriozkin, Mualem (2018)) has not been verified and implemented so far.

2.3 Recap and conclusions on hysteretic models

In this section, we have described and reviewed hysteresis models with detailed equations and graphics. From the above review of models, we conclude that hysteresis models of Doughty (2007) and Beriozkin, Mualem (2018) are respectively modifications of the original models of Mualem (1984) and Mualem (1974), where the modifications take into account the non-wetting phase entrapment in the hysteresis loops. The non-wetting phase entrapment can be represented in a hysteretic model by different formulas, such as Land's formula (Land (1968)), the linear law of Mualem (Mualem (1974)), or Aissaoui's formula (Aissaoui (1983)). We think that the representation of the non-wetting phase saturation only by the first turning point is based on invalid hypotheses. In fact, this representation does not take into account a higher order of scanning curves and how they can induce release of a fraction of trapped non-wetting phase. For example, taking a primary wetting curve departing from the main drying curve produces a residual gas saturation of $S_{gr,1}^{\Delta}$; after the second drying curve a third wetting curve may produce a residual gas saturation of $S_{gr,2}^{\Delta} \leq S_{gr,1}^{\Delta}$, which is not taken into account. Even a portion of entrapped non-wetting phase was released due to the second drying path, the model kept the first $S_{gr,1}^{\Delta}$ entrapment value in order to avoid the pumping errors.

The empirical model presented above did not take into account the rate of the process, which is an important factor for fluid transport in porous media as described by Topp et al. (1967). Hannes et al. (2016) proposed three classifications of temporal dynamics of soil water retention: the first class is the non-equilibrium process where fast changes may occur in the water retention; the second class is a quasi-equilibrium process, where relatively slow changes in the water retention are pursued by the fluid redistribution; the third class is the temporal dynamics of soil structures, where the variation of pore structure may occur due to a chemical or mechanical process. Using laboratory data of the soil water retention at different flow processes, they showed that the conceptual models of Parker, Lenhard (1987), Mualem (1984), and Poulovassilis, Kargas (2000), failed to reproduce the hysteresis of a non-equilibrium process, especially when the rate of changes in water saturation is high.

In case the capillary entry pressure ($P_{c,e}$) is considered in the constitutive relations S_l-P_c-$k_{r,l}$-$k_{r,g}$ of the Van Genuchten-Mualem model (Eqs. (24), (20), and (21)), the representation of hysteresis in the iTOUGH2 code depends on the second primary variable chosen for solving the compositional two-phase flow equations (Amri et al. (2022)). This second primary variable is either gas saturation or capillary pressure. When gas saturation is used as a primary variable, the release of trapped non-wetting phase in iTOUGH2 is activated by assuming numerically a high saturation at a specified time step. Otherwise,

when the capillary pressure is used as a primary variable, the release of trapped non-wetting phase is straightforward (release when $P_c > P_{c,e}$). However, the present study does not take into account $P_{c,e}$, and its influence on non-wetting phase trapping is beyond the scope of this paper.

3 Comparative study of water retention hysteresis models

In the previous section we have analysed and reviewed different hysteresis models one by one; in this section we proceed with inter-comparisons of these hysteresis models in terms of hysteretic water retention curves. Inter-comparisons introducing measured hysteretic relative permeability to liquid and gas were not possible because these permeability data were missing for the five materials studied (only saturation-capillary pressure data were available).

Several studies have focused on comparisons of hysteresis models (Pham et al. (2005), Zhang et al. (2014), and Terleev et al. (2018)). These studies have showed that the conceptual hysteresis models, which are based on the main wetting and drying curves (and not on the intermediate scanning curves) for their calculations, are simple and more accurate for predicting the scanning curves than the empirical models. Compared to these conceptual models, the empirical models require more difficult calibrations of additional parameters, using more detailed experimental data on intermediate turning points.

On the other hand, the review studies cited just above did not cover all conceptual hysteresis models, and they did not include more recent concepts like non-wetting phase entrapment phenomena. These were taken into account in the more recent studies of Doughty (2007) and Beriozkin, Mualem (2018)).

In this section, we test the performance of the five hysteresis models discussed in *Section 2* in reproducing the hysteresis data of different porous materials (Sands, Cement, Bentonite) collected from the literature.

3.1 Data preparation and comparison criteria

The characteristics of hysteresis data of five porous materials collected from the literature are presented in Table (1). The experimental data of water content $\theta(P_c)$ are normalized to $S_l(P_c)$ via equation (29):

$$S_l = \frac{\theta - \theta_r}{\theta_s - \theta_r} \tag{29}$$

The experimental data of the water retention curve measured for incremental relative humidity (RH), i.e. $S_l(RH)$, are transformed into $S_l(P_c)$ by using Kelvin's equation (30):

$$P_c = \frac{\rho_l RT}{M_l} ln(RH) \tag{30}$$

where R = 8.314 $J \times K^{-1}$ $J \times mol^{-1}$ is the universal gas constant, $T(K)$ is the absolute temperature and M_l is the molar mass of liquid water molecule $(kg \times mol^{-1})$.

Material	References	Type of soil	Scanning curves
1	Terleev et al. (2018)	Dune sand	1st wetting
2	Baroghel-Bouny (2007)	Paste(CEM I)	1st wetting
			2nd drying
3	Huang et al. (2005)	Compacted Sand	1st wetting
			2nd drying
			3rd wetting
4	Qiao et al. (2021)	Bentonite MX80	1st wetting
5	Lins et al. (2007)	Hostun sand	1st wetting
			2nd drying
			3rd wetting

Table 1: Hydraulic properties of different porous materials studied.

First, the Van Genuchten - Mualem model (Van Genuchten (1980)) is fitted to experimental main wetting and drying curves. We make the choice of $S_{ls,d} = S_{ls,w}$ in the fitting procedure of the main curves by equation (7) for the hysteresis models Mualem 1974, Mualem 1984, and Haverkamp et al. 2002. Secondly, the hysteresis models are used to predict the scanning curves based on an iterative solution for scanning curves equations of each model. The goodness of fit of measured scanning points is evaluated using the Mean Absolute Error (MAE) defined by equation (31) :

$$MAE = \frac{1}{n} \sum_{i=0}^{n} |S_i - \tilde{S}_i| \tag{31}$$

where S_i, $\tilde{S}_i$ are the measured and predicted values of water saturation, and n is the number of measured data points. We define $MAE(N, p - k)$ as the mean absolute error of the kth measurement curve of the Nth scanning curve at the path $p \in \{w, d\}$.

3.2 Results and discussions

Figures (8, 9, 10, 11, 12) present the scanning curves predicted by the five hysteresis models, showing the MAE value for each scanning curve above each plot. The global MAE for each material and for each hysteresis model is presented in Table (2) in order to analyze the different mismatches between the models and data.

From the comparison of the values of MAE, we can conclude that all hysteresis models represent well the tendencies of scanning loops, except the Haverkamp et al. 2002 model which fails to predict the main wetting branches

N°	Mualem 1974	Mualem 1984	Haverkamp 2002	Doughty 2007	B&M 2018
1	0.05737	0.05738	**0.04148**	0.05656	0.06040
2	0.02511	0.03221	0.24811	0.05723	**0.02397**
3	0.02889	0.05733	0.23982	0.08832	**0.02799**
4	0.04069	0.04066	0.04322	**0.04062**	0.04062
5	0.02472	**0.01998**	0.15304	0.05887	0.02156
Mean	0.03535	0.04151	0.14513	0.06032	**0.03491**

Table 2: MAE results for the scanning curves fit of each material's experimental data by the five hysteresis models. The column N° refers to the number of the porous material as presented in Table (1).

for all materials (except material N° 4). The Mualem 1974 and Mualem 1984 models share the same first drying curve, but the Mualem 1974 model exhibits better results than Mualem 1984 for higher order scanning curves (e.g., materials N° 2, 3).

The Doughty 2007 model is a modification of the Mualem 1984 model by introducing a new wetting curve, determined after a reversal point from main drying to first wetting. The Doughty 2007 model presents a high error compared to the Mualem 1984 model, and therefore the introduction of non-wetting phase entrapment saturation enhances the Mualem 1974 model, but not the Mualem 1984 model.

Finally, the Beriozkin and Mualem 2018 model is slightly better, particularly compared to Haverkamp et al. 2002 and Doughty 2007 based on mean MAE values in Table (2), looking only at the first 2 digits; but more importantly, the Beriozkin and Mualem 2018 model gives an explicit formulation of the saturation of scanning curves, without the need for iterative solution of the equations representing the scanning curves, which is an advantage over the other models (Mualem 1974, Mualem 1984, Haverkamp et al. 2002, and Doughty 2007).
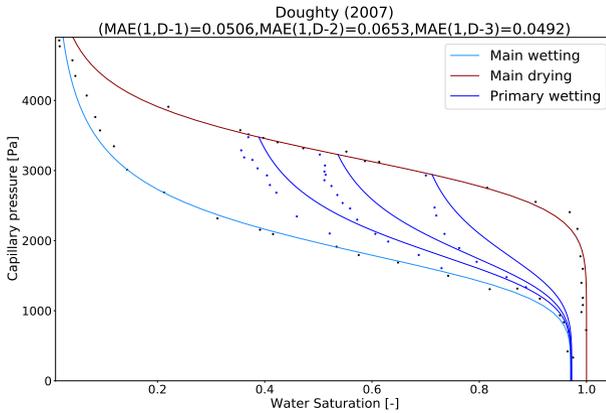
(a)

(b)

(c)

(d)

(e)
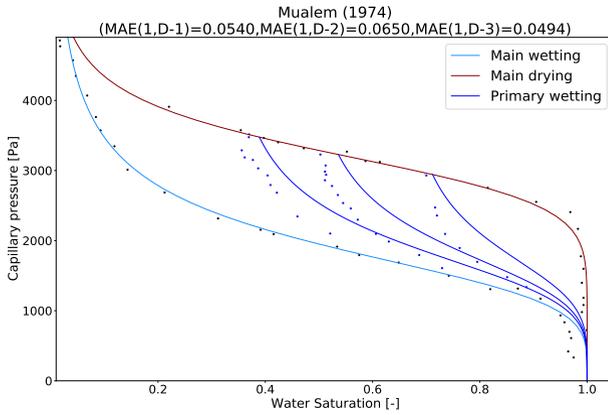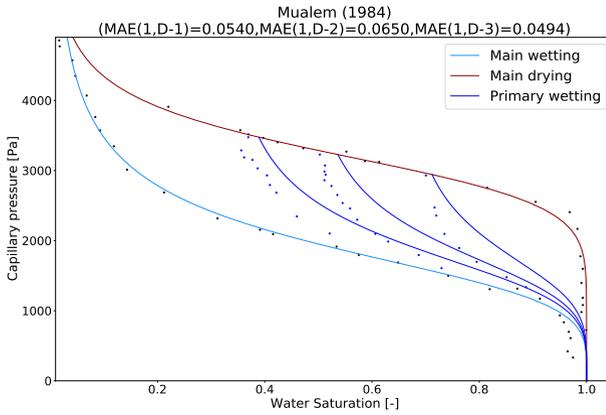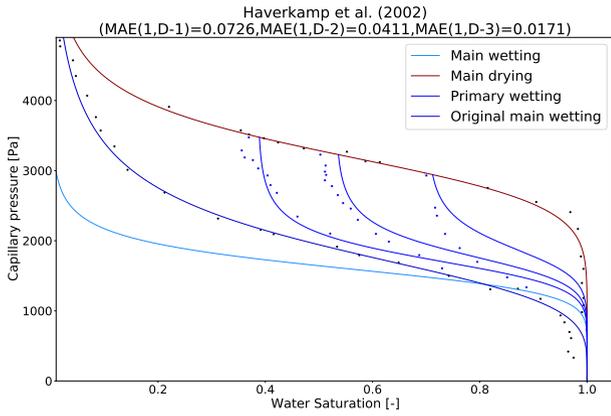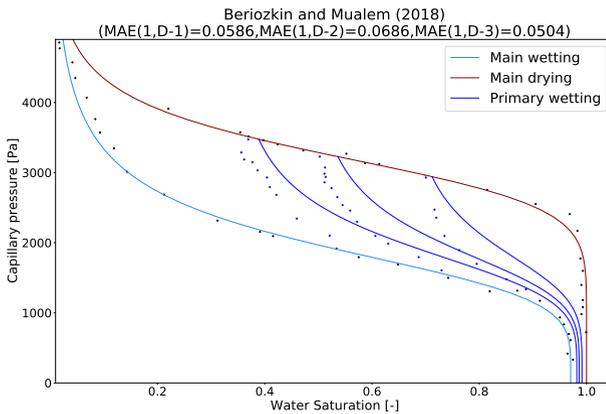
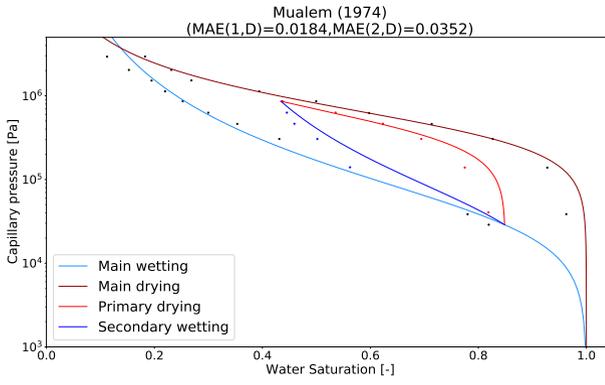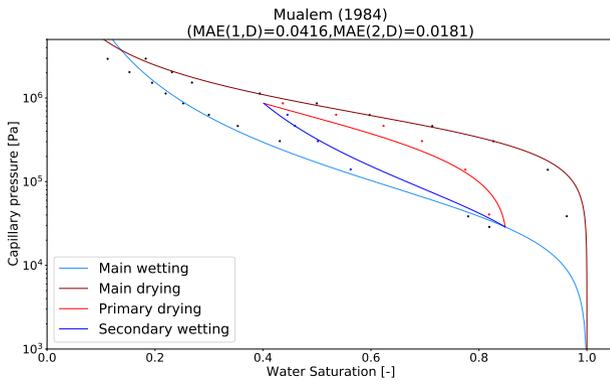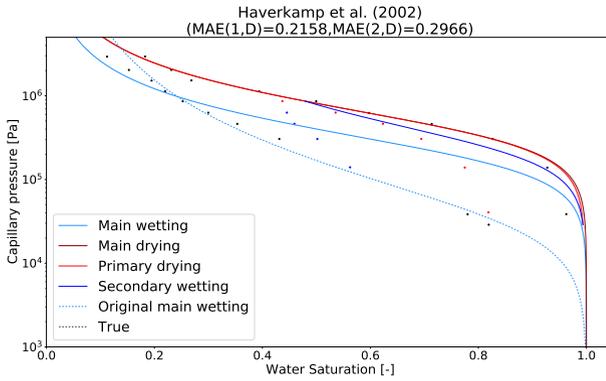**Figure 8**: Fitted main wetting and main drying curves to the Dune Sand (material $N°$ 1) data from Terleev et al. (2018), and three predicted primary wetting scanning curves departing from the main drying branch, according to the five hysteresis models (one model per subfigure, respectively, from (a) to (e)).
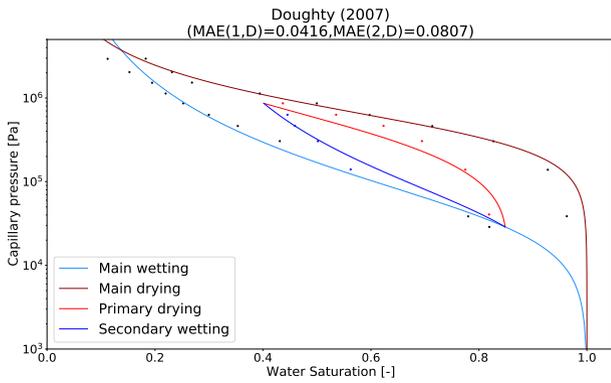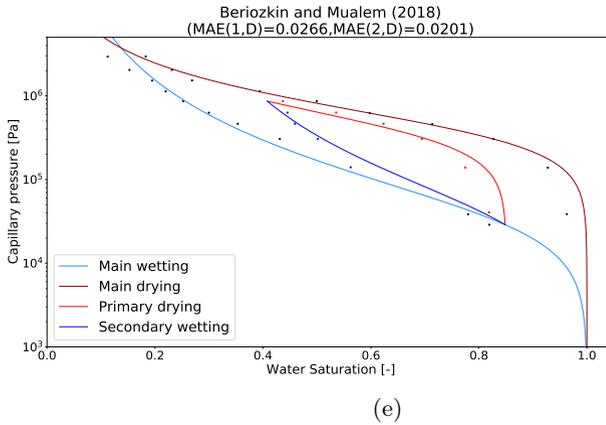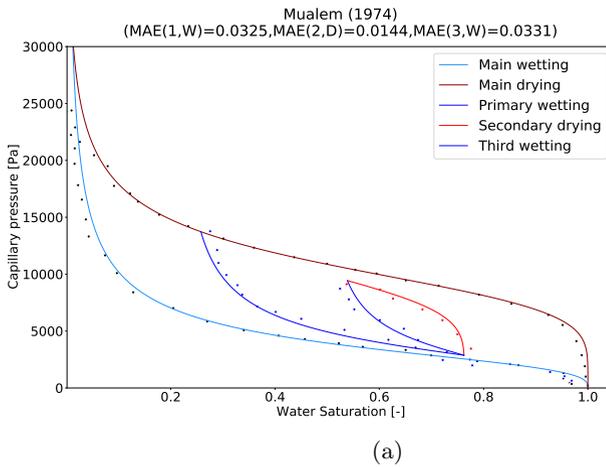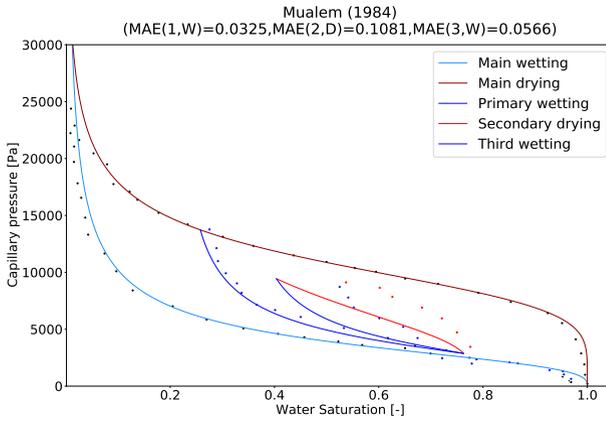
(a)

(b)

(c)

(d)

(e)

Figure 9: Fitted main wetting and main drying curves to the Cement Paste CEM I (material N° 2) data from Baroghel-Bouny (2007), and predicted first wetting scanning curve and second drying curve according to the five hysteresis models (one model per subfigure, (a) to (e)).
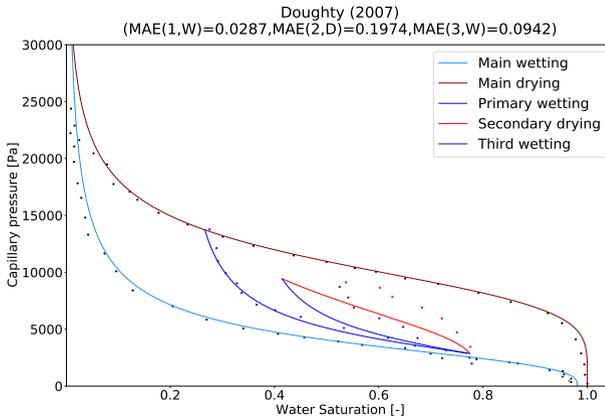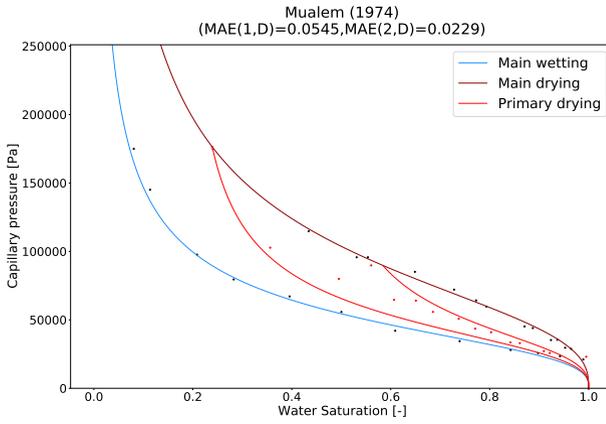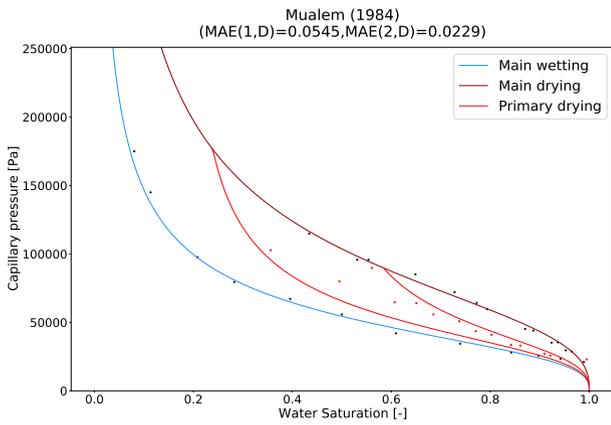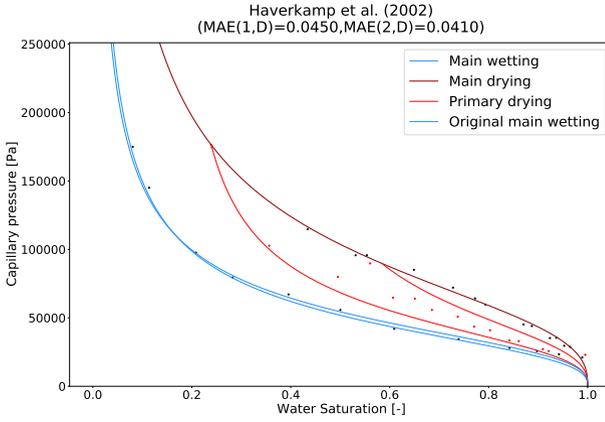

(a)

(b)

(c)

(d)

(e)
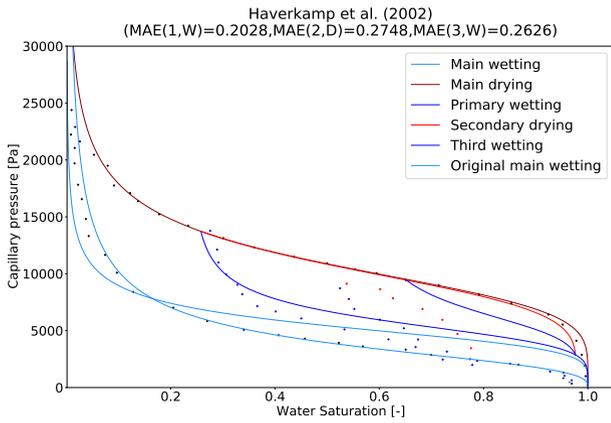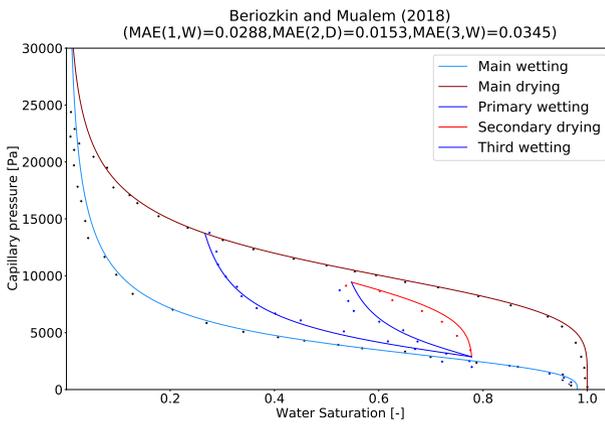
Figure 10: Fitted main wetting and main drying curves to the Compacted Sand (material $N°$ 3) data from Huang et al. (2005), and predicted scanning curves according to the five hysteresis models (one model per subfigure, from (a) to (e)).

(a)

(b)

(c)

(d)

(e)
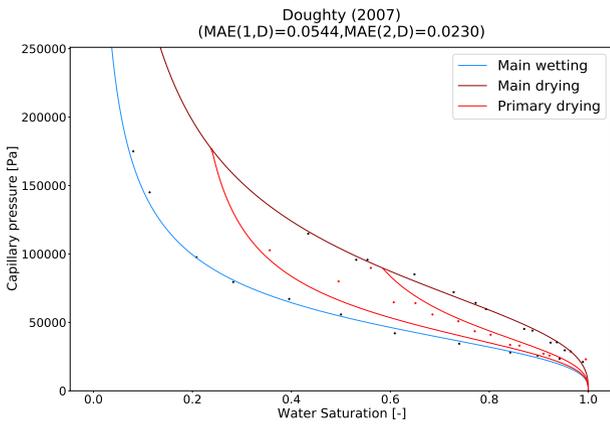
Figure 11: Fitted main wetting and main drying curves to the Bentonite MX80 (material $N°$ 4) data from Qiao et al. (2021), and predicted first wetting scanning curves according to the five hysteresis models (one model per subfigure, from (a) to (e)).
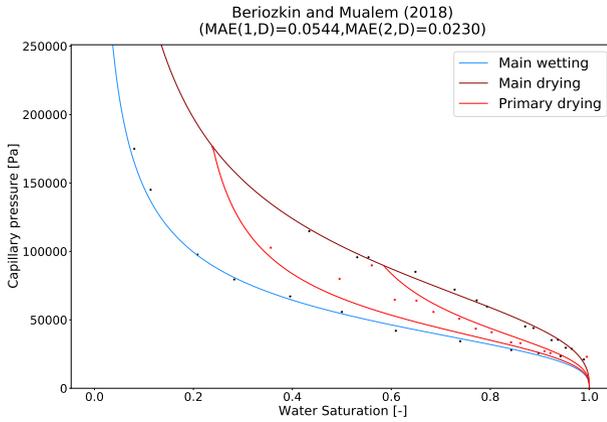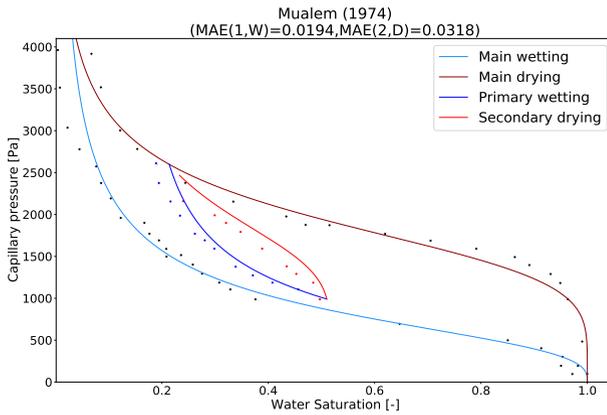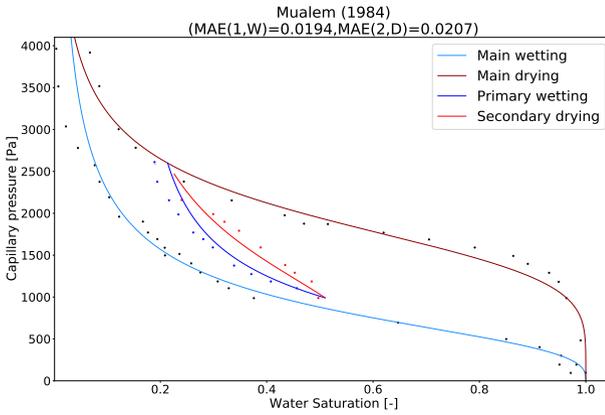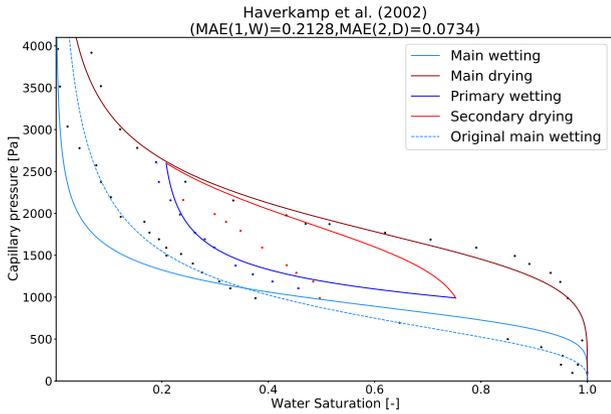

(a)

(b)

(c)

(d)

(e)
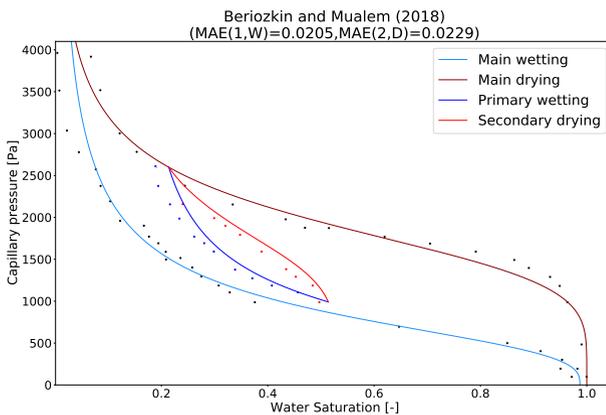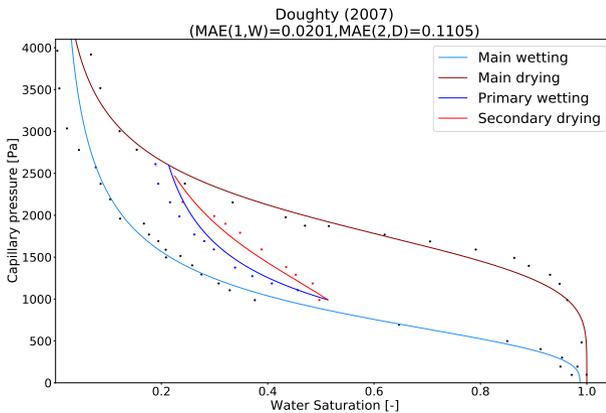
Figure 12: Fitted main wetting and main drying curves to the Hostun Sand (material $N°$ 5) data from Lins et al. (2007), and predicted first wetting curve and second drying scanning curve according to the five hysteresis models (one model per subfigure, from (a) to (e)).

.

4 Application: simulation of a 2-phase flow laboratory experiment emulating CO2 trapping with and without hysteresis

To study the effect of hysteresis on the behavior of two-phase flow systems, we have tested a constitutive model with and without hysteresis on the intermediate-scale laboratory experiments conducted by Trevisan et al. (2014).

The experiments involve the injection of surrogate fluids in order to mimic the behavior of the supercritical scCO2-brine system at the reservoir scale. Despite some differences in the input parameters between our modeling and theirs, we will compare our simulation results with some experimental data, and we will then discuss the effect of hysteresis on non-wetting plume migration.

4.1 The laboratory experiment of Trevisan et al. 2014

The sand aquifer was initially saturated with water, the wetting fluid. The experiment involved injection of a non-wetting fluid (Soltrol-220) into a rectangular two-dimensional slab of Sand 40/50 (the "aquifer"), with internal dimensions (L×W×H) equal to (91.4× 5.6× 61 cm^3) with an inclination angle of 2° (Figure 13). The right boundary of the aquifer was at equilibrium with a hydrostatic pressure. The well injection was placed on the left boundary of the aquifer. It consisted of a vertical PVC pipe with an internal diameter of 2.3 cm and a vertical length of 11 cm. For more details on this laboratory experiment, see Trevisan et al. (2014) and Cihan et al. (2017).

In our simulation of the experiment, we used a uniform grid with mesh size of 0.5 cm × 0.5 cm to represent the 2D domain shown in Figure (13). Our simulation consisted of two stages: a first stage of Soltrol-220 injection at a rate of 0.7ml/min during 5.5 h, followed by a second stage of spontaneous redistribution of the injected fluid during 15 more days.
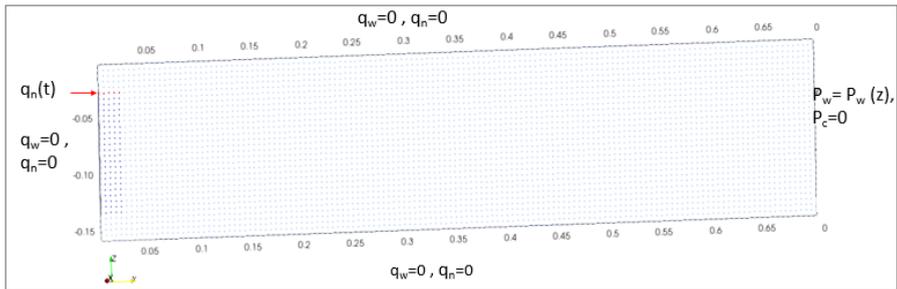
Figure 13: Schematic representation of the 2D domain and boundary conditions corresponding to the laboratory experiment of Trevisan et al. (2014) as simulated in the present paper.

.

4.2 Hydraulic properties and hysteretic models used

In the present work, the measured data of Sand 40/50 of water retention curves are fitted using the Van Genuchten model as shown in Figure (14). We tested two scenarios in the fitting procedure. The first one consists in taking into account the non-wetting phase entrapment phenomenon by considering

Table 3: Adjusted hydraulic parameters for the Sand 40/50. Scenario 1 is for $S_{w,max}$ as a free parameter. Scenario 2 is for fixed $S_{w,max} = 1.0$.

| Scenario	n_w	$\alpha_w\ [Pa^{-1}]$	$S_{w,max}$	$S_{w,r}$	n_d	$\alpha_d\ [Pa^{-1}]$	$S_{d,max}$	$S_{d,r}$
1	2.95	3.89×10^{-3}	0.8431	0.0073	3.91	1.76×10^{-3}	1.00	0.0097
2	2.56	5.26×10^{-3}	1.0	0	3.91	1.76×10^{-3}	1.00	0.0097

$S_{w,max}$ as a free parameter in the fitting procedure. The second one consists in neglecting the non-wetting phase entrapment saturation by constraining $S_{w,max}$ to 1.0. The fitted parameters with the two scenarios are given in Table (3).

The hysteresis models of Beriozkin, Mualem (2018) and Doughty (2007) are used here to describe the mechanism of non-wetting phase entrapment saturation (Figure (14)). The Mualem (1974) model is used to describe the hysteresis phenomenon without non-wetting phase entrapment. The intrinsic permeability is $k = 6.43\times10^{-11}[m^2]$ and the porosity is $\phi = 0.35$.
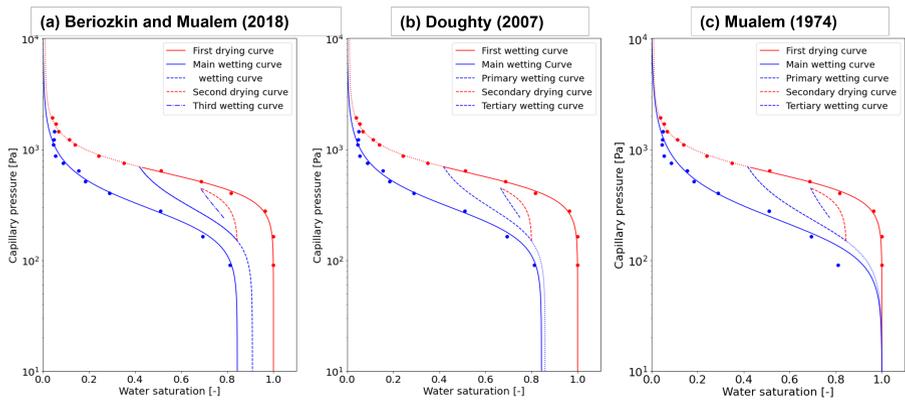
Figure 14: Illustration of the hysteresis effect on retention curve properties of Sand 40/50. Scanning loops are calculated with different models. (a) Beriozkin, Mualem (2018). (b) Doughty (2007). (c) Mualem (1974).

Note that there are no data points for the scanning curves, and they are entirely predicted by the afore-mentioned models. The main difference between the models of Doughty (2007) and Beriozkin, Mualem (2018) is the amount of non-wetting phase entrapment saturation at the end of the first wetting scanning curve. This difference is mainly related to the representation of the non-wetting phase entrapment saturation. For example, the Beriozkin, Mualem (2018) model uses a linear model to represent the relation $S_{gr} - S_{tp}$ which gives a non-wetting phase entrapment saturation of 0.105 when the turning point saturation $S_{tp} = 0.41$. However, the Doughty (2007) model uses the formula

of Land (1968), which gives a non-wetting phase entrapment saturation of 0.147 for the same turning point $S_{tp} = 0.41$. This difference between the two formulae concerning the $S_{gr} - S_{tp}$ relationships is presented in Figure (15) in comparison with experimental data of Sand 40/50 from Trevisan et al. (2014). The fit of experimental data of $S_{gr} - S_{tp}$ reveals that the Aissaoui's formulation (Aissaoui (1983)) is in good agreement with measured data. This observation is also in agreement with Suzanne et al. (2003) and Pentland et al. (2010).
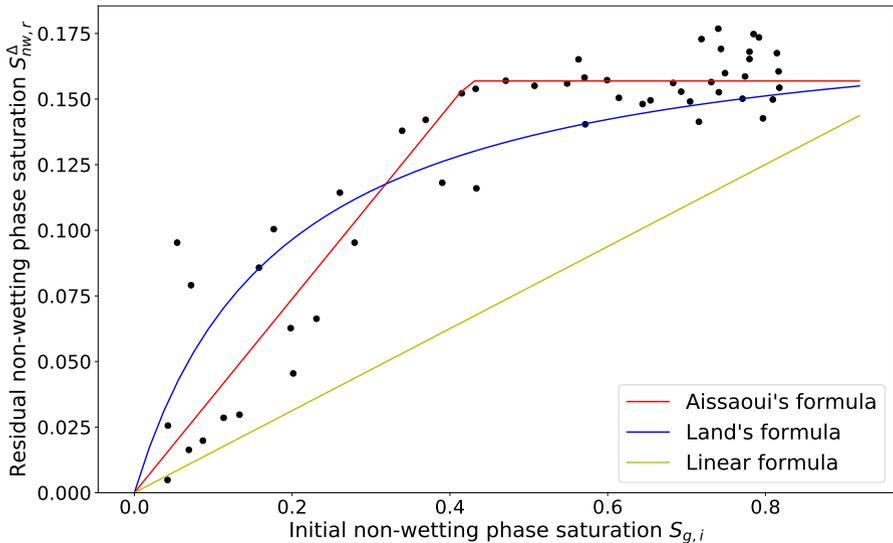
Figure 15: Comparison of non-wetting phase entrapment representations according to the Aissaoui, the linear, and the Land formulae. The points (black dots) represent experimental entrapment data for the Sand 40/50 from Trevisan et al. (2014).

4.3 Simulation results and discussion

In this section, we present a comparison between the simulation results obtained respectively with (i) a non-hysteretic model, (ii) the hysteretic Beriozkin, Mualem (2018) model, (iii) the hysteretic Doughty (2007) model, and (iv) the hysteretic Mualem (1974) model. First, the effect of hysteresis is discussed by using the Beriozkin, Mualem (2018) model. Secondly, the effect of non-wetting phase entrapment is discussed by comparing Doughty (2007) and Mualem (1974) models. Finally, a comparison between the simulation results and the measured saturations from the laboratory experiment is presented.

4.3.1 Effect of different hysteresis models on the distribution of injected non-wetting fluid during post-injection

As presented in section 3, the Beriozkin, Mualem (2018) hysteretic model presents a good agreement with experimental data of different porous materials types, and we focus mainly on this hysteretic model for simulations of the two-phase flow laboratory experiment. We also compare with simulations obtained with another hysteresis model (Doughty (2007)), and with simulations without hysteresis. We choose here to implement these two-phase hysteretic models, as well as the non-hysteretic model, with the iTOUGH2 code (Finsterle et al. (2017)).

Figure (16) shows the 2D distribution of the non-wetting phase (Figure 16.a) and the curve number or index number (Figure 16.b) at different post-injection times. At the end of the injection, a new index curve equal to 2 starts to appear in the vicinity of the injection well, corresponding to the first imbibition path in the $P_c - S_l$ relationships. At the same time the region of drainage ($icurve = 1$) starts migrating towards the other boundary.
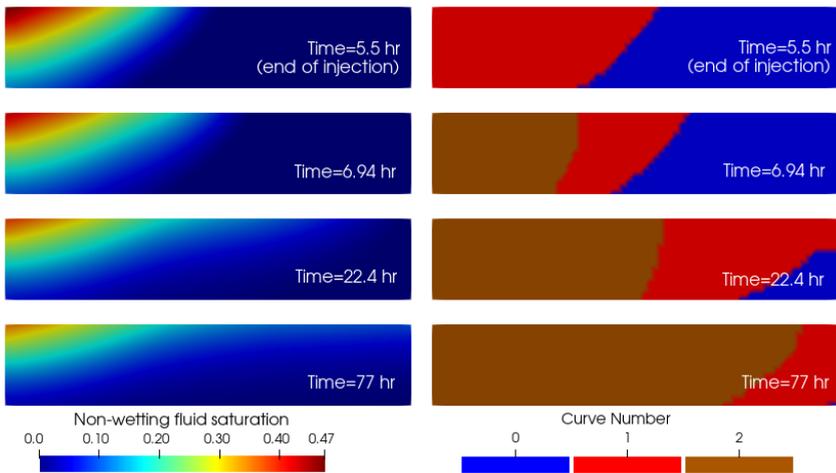
Figure 16: (a) Simulated 2D distribution of the non-wetting fluid saturation at different times by Beriozkin, Mualem (2018) hysteresis model. (b) Flow reversal index numbers where $icurve = 0$ designates fully saturation state ($S_l = 1$), $icurve = 1$ designates main drying curve, and $icurve = 2$ designates the first wetting curve.

Figure 17 presents a comparison between simulation results without a hysteretic model and with the hysteretic Doughty (2007) model. The amount of non-wetting phase saturation is clearly different between the two models. The hysteresis model simulates a higher non-wetting phase at the vicinity of the well

injection. The imbibition process near the injection well affects the permeabil-
ity of the non-wetting phase and leads to a higher non-wetting phase saturation
than the non-hysteretic model which consists of much higher movement of
the injected fluid during time. By the end of the simulation (at time $t = 77$
hours) a significant difference in the non-wetting phase saturation between
the two models is observed. This difference is due to the non-wetting phase
entrapment which leads to small permeability in the imbibition region. The
same observation was reported by Zhao et al. (2014) where the re-imbibition
curves corresponding to the first wetting curve of relative permeability where
under the main drainage curve. From the results shown in figures (16.a) and
(17.b), no big differences are observed between Beriozkin, Mualem (2018) and
Doughty (2007) models.

Figure 17: Simulated 2D distribution of the non-wetting fluid (Soltrol-220)
saturation at different times ($t = 5.5, 6.94, 22.4, 77\ hours$). (a) Results from
the model without hysteresis. (b) Results with the hysteretic model of Doughty
(2007).

The effect of neglecting Soltrol-220 entrapment saturation in the hysteresis
models is shown in figure (18) where the Doughty (2007) model is compared to
the Mualem (1974) model using respectively the parameters of scenario 1 and
scenario 2 as explained above (see table 3). By the end of the post-injection
period, the Mualem (1974) and Beriozkin, Mualem (2018) models simulate the
same evolution of the non-wetting fluid. The difference between the two mod-
els becomes more significant as time increases ($t > 6.94\ h$). In fact, according
to the Mualem (1974) model a small non-wetting phase remains in the system
compared to the Beriozkin, Mualem (2018) model, especially near the region
where the imbibition process occurred. This may be due to the higher perme-
ability of the hysteretic model without Soltrol-220 entrapment, and also, to
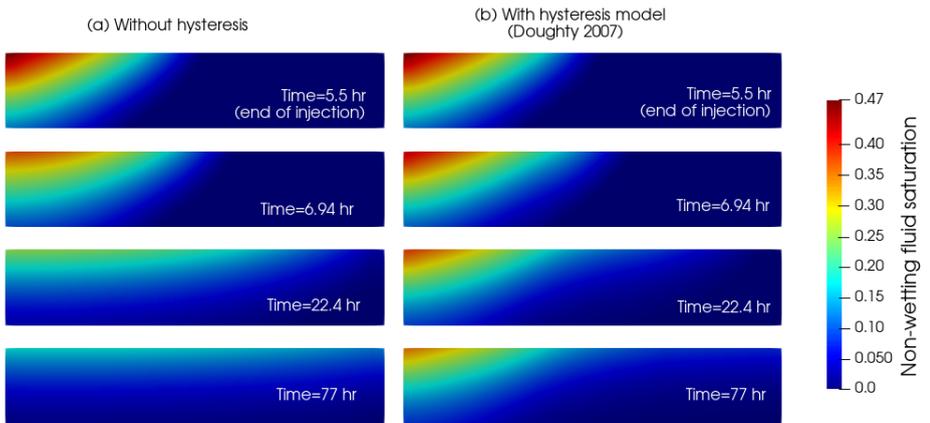the easier migration of the non-wetting phase in the absence of entrapment.
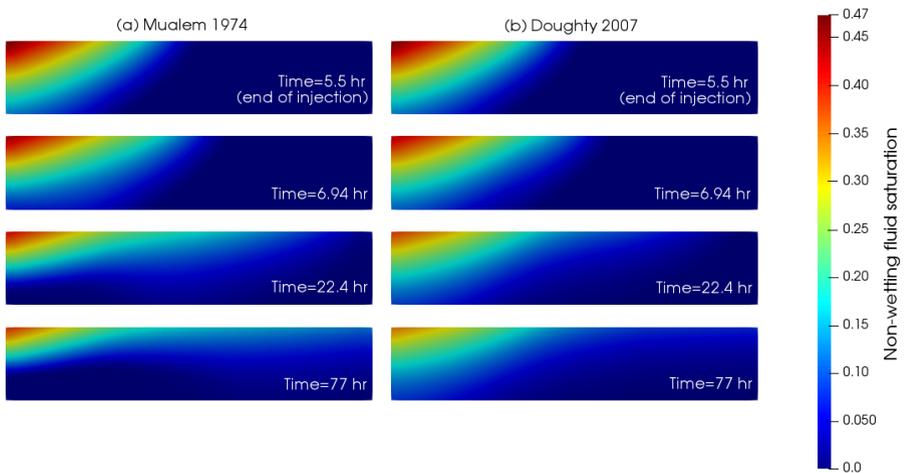
Figure 18: Simulated 2D distribution of the non-wetting fluid (Soltrol-220) saturation at different times ($t = 5.5, 6.94, 22.4, 77$ *hours*). (a) Results with the hysteretic model of Mualem (1974). (b) Results with the hysteretic model of Doughty (2007).

In the light of these simulation results, hysteresis may play a significant role in the migration of the non-wetting phase. This result is coherent with the shapes of scanning curves compared to the main drainage (Figure 16.b). In fact, the scanning curve presents a lesser capacity of wetting phase retention compared to the main drainage. This increases the retention of the non-wetting fluid. The non-wetting phase entrapment phenomenon accentuates the high retention of the non-wetting phase, leading to higher quantities of non-wetting fluid in the system.

4.3.2 Discussions on simulated vs. experimental saturations with and without hysteresis

In this subsection, the simulation results are discussed and compared with saturation measurements from the laboratory experiment of Trevisan et al. (2014). Due to uncertainties in the input parameters, the present simulation results may not be in agreement with the experimental observations, but nevertheless, the impact of the hysteresis model is clearly observed in our simulations, as

in those of Cihan et al. (2017). Qualitatively, the observed differences between Cihan et al. (2017) and our simulated results include the following:

- The obtained spatial distribution of the non-wetting fluid $S_{nw}(x,y)$ indicates that the injected non-wetting fluid does not go upwards in our simulation, whereas it does in the simulation of Cihan et al. (2017);
- We have indications that, probably for the same reason, the vertical position $z_c(t)$ of the center of mass of the non-wetting plume does not go upwards in our simulation, whereas it does in the simulation of Cihan et al. (2017).

These differences between our simulations and those of Cihan et al. (2017) may be due to the following facts:

- The inclination of the flow domain is possibly different;
- The hydraulic properties for our simulation are possibly different from those of Cihan et al. (2017);
- The densities of the fluids are not exactly the same in our simulations and those of Cihan et al. (2017).

Figures (19) and (20) compare the picture taken during the end of the post-injection period and the simulation results. The hysteresis model presents the observed migration plume better than the non-hysteretic model. Uncertainties in the input parameters may affect the simulation results but the trends are clear enough to confirm the accuracy of the hysteretic model to represent the migration of non-wetting phase during a post-injection period.

In order to quantify the amount of the difference between hysteretic and non-hysteretic models, Trevisan et al. (2014) used experimental saturation data measured by the X-Ray attenuation method to calculate spatial moments of the non-wetting plume, based on the non-wetting saturation distribution $S_{nw}(x,z)$. In particular, the center of mass coordinates $x_c(t)$ and $z_c(t)$ were analyzed. However, because experimental data are not entirely available from the experimental study of Trevisan et al. (2014) and the simulation study of Cihan et al. (2017), this type of spatial moments analysis was not possible in our simulation study due, seemingly, to lack of information on some physical parameters of the experiment.
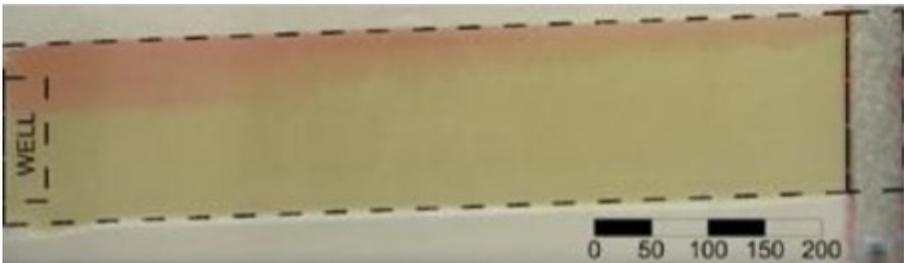

Figure 19: Picture taken during the experiments at the end of the recovery period $t = 15\ days$ from Cihan et al. (2017).

(a) Beriozkin & Mualem 2018
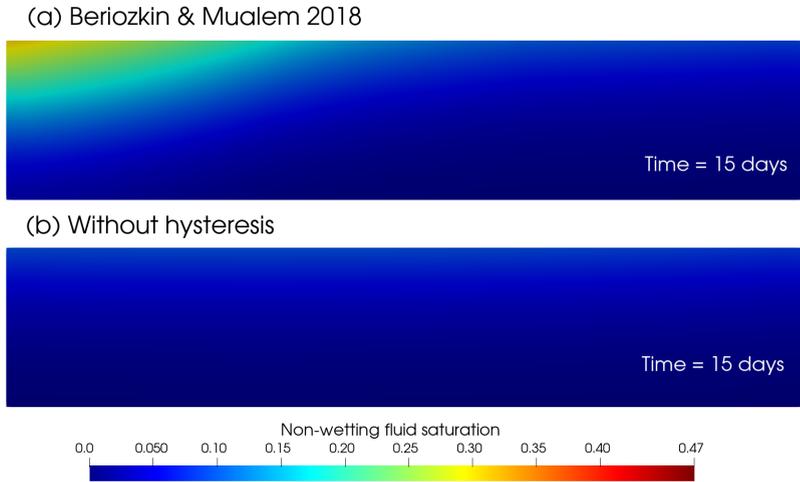

(b) Without hysteresis

Figure 20: Simulated 2D distribution of non-wetting fluid saturation at the end of the post-injection period $t = 15$ *days*. (a) Result with the hysteretic model of Beriozkin, Mualem (2018). (b) Result with the non-hysteretic model.

From the 2D simulations results, we can conclude that the hysteresis models are more accurate to predict the non-wetting plume migration in the post-injection period. The comparison of hysteresis models also showed that neglecting the non-wetting phase entrapment may affect the simulation results at large times.

5 Conclusions

In this study, we have presented a detailed review, and a quantitative assessment, of several of the most important and representative conceptual models for hysteretic two-phase flow in porous media. Model equations and hypotheses were analyzed in detail, with comments on the required solution steps in the presence of turning points due to wetting-drying cycles. Globally, our survey indicates that the hysteretic models of two-phase flow agree fairly well with the experimental data, compared to the non-hysteretic models.

Given the goodness of fit of the Beriozkin, Mualem (2018) model to experimental data, and its explicit calculation of saturation scanning curves, and also, its taking into account of the non-wetting phase (gas) entrapment, it can be considered as a good candidate for implementing hysteresis in 2-phase flow simulations. The models of Mualem (1974) and Mualem (1984) also give good results on experimental data but without representing the gas entrapment phenomenon. Finally, the model of Haverkamp et al. (2002) gives the least accurate results among the models that we have selected for this review with respect to the experimental data that we have analyzed and simulated.

Our simulation results highlight the ability of hysteretic models to reproduce the post-injection non-wetting plume distribution in the intermediate-scale laboratory experiment, compared to non-hysteretic simulations. Neglecting the non-wetting phase entrapment may also affect the simulation results. The modeling of this experiment, where a non-wetting fluid is injected in a reservoir initially saturated with a wetting fluid, confirms the necessity of considering hysteresis in modeling such multiphase flow systems. The Beriozkin, Mualem (2018) model is found to be the most adequate to model hysteresis due to its advantages of reproducing well the experimental data, and relative simplicity of implementation. Furthermore, it is expected that this model is the best one in terms of CPU times, because it solves explicit equations for calculating hysteretic scanning curves.

Further developments should take into account, in combination with hysteretic effects, the phenomenon of capillary trapping of the non-wetting phase (e.g., hydrogen gas), and also, the existence of a capillary entry pressure which can induce a gas entry pressure threshold: see Amri et al. (2022) for a recent sensitivity study of water-gas flows with and without entry pressure.

References

Aissaoui A. Etude théorique et expérimentale de l'hystérésis des pressions capillaries et des perméabilités relatives en vue du stockage souterrain de gaz. PhD thesis, Ecole des Mines de Paris, Paris, France. 1983.

Albers B. Modeling the hysteretic behavior of the capillary pressure in partially saturated porous media: a review // Acta Mechanica. 2014. 225, 8. 2163–2189.

Amri A, Saâdi Z, Ababou R. Parametric Sensitivity to Capillary Entry Pressure in Two-Phase Water-Gas Flow Models: Deep Geologic Disposal of Radioactive Waste // Transport in Porous Media. 2022. 145. 13–43.

Baroghel-Bouny V. Water vapour sorption experiments on hardened cementitious materials: Part I: Essential tool for analysis of hygral behaviour and its relation to pore structure // Cement and Concrete Research. 2007. 37, 3. 414–437. (Note: Cementitious materials as model porous media: nanostructure and transport processes).

Beriozkin A, Mualem Y. Comparative analysis of the apparent saturation hysteresis approach and the domain theory of hysteresis in respect of prediction of scanning curves and air entrapment // Advances in Water Resources. 2018. 115. 253–263.

Braddock RD, Parlange J-Y, Lee H. Application of a soil water hysteresis model to simple water retention curves // Transport in porous media. 2001. 44, 3. 407–420.

Cihan A, Birkholzer J, Trevisan L, Gonzalez-Nicolas A., Illangasekare T. Investigation of representing hysteresis in macroscopic models of two-phase flow in porous media using intermediate scale experimental data // Water Resources Research. 2017. 53, 1. 199–221.

Doughty C. Modeling geologic storage of carbon dioxide: Comparison of non-hysteretic and hysteretic characteristic curves // Energy Conversion and Management. 2007. 48, 6. 1768–1781. Geologic Carbon Sequestration and Methane Hydrates Research from the TOUGH Symposium 2006.

Doughty C. User's guide for hysteretic capillary pressure and relative permeability functions in TOUGH2. 2013.

Feng M, Fredlund DG. Hysteretic influence associated with thermal conductivity sensor measurements // Proceedings from Theory to the Practice of Unsaturated Soil Mechanics in Association with the 52nd Canadian Geotechnical Conference and the Unsaturated Soil Group, Regina, Sask. 14, 2. 1999. 14–20.

Finsterle S, Commer M, Edmiston JK, Jung Y, Kowalsky MB, Pau GSH, Wainwright HM, Zhang Y. iTOUGH2: A multiphysics simulation-optimization framework for analyzing subsurface systems // Computers Geosciences. 2017. 108. 8–20. TOUGH Symposium 2015: recent enhancements to the TOUGH family of codes and coupled flow and geomechanics processes modeling.

Hannes M, Wollschläger U, Wöhling T, Vogel H-J. Revisiting hydraulic hysteresis based on long-term monitoring of hydraulic states in lysimeters // Water Resources Research. 2016. 52, 5. 3847–3865.

Haverkamp R, Reggiani P, Ross PJ, Parlange J-Y. Soil water hysteresis prediction model based on theory and geometric scaling // Environmental mechanics: Water, mass and energy transfer in the biosphere. 2002. 129. 213–246.

Hesse MA, Woods AW. Buoyant dispersal of CO2 during geological storage // Geophysical Research Letters. 2010. 37, 1.

Huang H-C, Tan Y-C, Liu C-W, Chen C-H. A novel hysteresis model in unsaturated soil // Hydrological Processes. 2005. 19, 8. 1653–1665.

Kaluarachchi JJ, Parker JC. Multiphase flow with a simplified model for oil entrapment // Transport in porous media. 1992. 7, 1. 1–14.

Krevor SCM, Pini R, Li B, Benson SM. Capillary heterogeneity trapping of CO2 in a sandstone rock at reservoir conditions // Geophysical Research Letters. 2011. 38, 15.

Land CS. Calculation of imbibition relative permeability for two- and three-phase flow from rock properties // Society of Petroleum Engineers Journal. 1968. 8, 02. 149–156.

Lenhard RJ. Measurement and modeling of three-phase saturation-pressure hysteresis // Journal of Contaminant Hydrology. 1992. 9, 3. 243–269.

Lenhard RJ, Parker JC. A model for hysteretic constitutive relations governing multiphase flow: 2. Permeability-saturation relations // Water Resources Research. 1987. 23, 12. 2197–2206.

Lenhard RJ, Parker JC, Kaluarachchi JJ. A model for hysteretic constitutive relations governing multiphase flow: 3. Refinements and numerical simulations // Water Resources Research. 1989. 25, 7. 1727–1736.

Lenhard RJ, Parker JC, Kaluarachchi JJ. Comparing simulated and experimental hysteretic two-phase transient fluid flow phenomena // Water Resources Research. 1991. 27, 8. 2113–2124.

Lenhard RJ, Parker JC, Van Genuchten MTh, Leij FJ, Lund LJ. Modeling multiphase fluid hysteresis and comparing results to laboratory investigations // Proc. Intl. Workshop on Indirect Methods for Estimating the Hydraulic Properties of Unsaturated Soils, edited by M. Th van Genuchten, FJ Leij, and LJ Lund, University of California, Riverside. 1992. 233–248.

Li XS. Modelling of hysteresis response for arbitrary wetting/drying paths // Computers and Geotechnics. 2005. 32, 2. 133–137.

Lins Y, Zou Y, Schanz T. Physical Modeling of SWCC for Granular Materials // Theoretical and Numerical Unsaturated Soil Mechanics. Berlin, Heidelberg: Springer Berlin Heidelberg, 2007. 61–74.

M'Jahad S. Impact de la fissuration sur les propriétés de rétention d'eau et de transport de gaz des géomatériaux: Application au stockage géologique des déchets radioactifs. 2012.

Mualem Y. A conceptual model of hysteresis // Water Resources Research. 1974. 10, 3. 514–520.

Mualem Y. A new model for predicting the hydraulic conductivity of unsaturated porous media // Water Resources Research. 1976. 12, 3. 513–522.

Mualem Y. A modified dependent-domain theory of hysteresis // Soil science. 1984. 137, 5. 283–291.

Mualem Y, Beriozkin A. General scaling rules of the hysteretic water retention function based on Mualem's domain theory // European Journal of Soil Science. 2009. 60, 4. 652–661.

Niemi A, Bodvarsson GS. Preliminary capillary hysteresis simulations in fractured rocks, Yucca Mountain, Nevada // Journal of Contaminant Hydrology. 1988. 3, 2. 277–291. Rapid and Far-Reaching Hydrologic Processes in the Vadose Zone.

Parker JC, Lenhard RJ. A model for hysteretic constitutive relations governing multiphase flow: 1. Saturation-pressure relations // Water Resources Research. 1987. 23, 12. 2187–2196.

Parlange J-Y. Capillary hysteresis and the relationship between drying and wetting curves // Water Resources Research. 1976. 12, 2. 224–228.

Pentland CH, Itsekiri E, Al Mansoori SK, Iglauer S, Bijeljic B, Blunt MJ. Measurement of Nonwetting-Phase Trapping in Sandpacks // SPE Journal. 03 2010. 15, 02. 274–281.

Pham HQ, Fredlund DG, Barbour SL. A study of hysteresis models for soil-water characteristic curves // Canadian Geotechnical Journal. 2005. 42, 6. 1548–1568.

Poulovassilis A. Hysteresis of pore water, an application of the concept of independent domains // Soil Science. 1962. 93. 405–412.

Poulovassilis A, Kargas G. A note on calculating hysteretic behavior // Soil Science Society of America Journal. 2000. 64, 6. 1947–1950.

Preisach F. Über die magnetische Nachwirkung // Zeitschrift für physik. 1935. 94, 5-6. 277–302.

Qiao Y, Tuttolomondo A, Lu X, Laloui L, Ding W. A generalized water retention model with soil fabric evolution // Geomechanics for Energy and the Environment. 2021. 25. 100205.

Raeesi B, Morrow NR, Mason G. Capillary Pressure Hysteresis Behavior of Three Sandstones Measured with a Multistep Outflow–Inflow Apparatus // Vadose Zone Journal. 2014. 13, 3. vzj2013.06.0097.

Rubin J. Numerical method for analyzing hysteresis-affected, post-infiltration redistribution of soil moisture // Soil Science Society of America Journal. 1967. 31, 1. 13–20.

Scott PS. Hysteretic effects on net infiltration // Advances in infiltration. 1983. 163–170.

Suzanne K, Hamon G, Billiotte J, Trocme V, others. Experimental relationships between residual gas saturation and initial gas saturation in heterogeneous sandstone reservoirs // SPE Annual Technical Conference and Exhibition. 2003.

Terleev V, Mirschel W, Nikonorov A, Ginevsky R, Lazarev V, Topaj A, others. Five models of hysteretic water-retention capacity and their comparison for sandy soil // MATEC web of conferences. 193. 2018. 02036.

Topp GC, Klute A, Peters DB. Comparison of water content-pressure head data obtained by equilibrium, steady-state, and unsteady-state methods // Soil Science Society of America Journal. 1967. 31, 3. 312–314.

Trevisan L, Cihan A, Fagerlund F, Agartan E, Mori H, Birkholzer JT, Zhou Q, Illangasekare TH. Investigation of mechanisms of supercritical CO2 trapping in deep saline reservoirs using surrogate fluids at ambient laboratory conditions // International Journal of Greenhouse Gas Control. 2014. 29. 35–49.

Van Genuchten MTh. A closed-form equation for predicting the hydraulic conductivity of unsaturated soils 1 // Soil Science Society of America Journal. 1980. 44, 5. 892–898.

Zhang Z. Modelling of sorption hysteresis and its effect on moisture transport within cementitious materials. 2014.

Zhang Z, Thiéry M, Baroghel-Bouny V. A review and statistical study of existing hysteresis models for cementitious materials // Cement and Concrete Research. 2014. 57. 44–60.

Zhao B, MacMinn CW, Huppert HE, Juanes R. Capillary pinning and blunting of immiscible gravity currents in porous media // Water Resources Research.

2014. 50, 9. 7067–7081.